

# Experimental investigation of the emergence of strain localization in geomaterials

Pierre Bésuelle  
Université Grenoble Alpes and CNRS  
Laboratoire 3SR

**ALERT Geomaterials school – Aussois – 6<sup>th</sup>-8<sup>th</sup> October 2016**



## P. Bésuelle, P. Lanatà

## 1 Introduction

[EAND] E.C. Ando, S.A. Hall, J. Desres, and P. Bésénelle. Experimental micromechanics: a virtual test on sand observed at the grain scale. *Geotech. Lett.*, 2(3):107–112, 2012.

[AIVH] E. Ando, S.A. Hall, G. Viggiani, J. Desres, and P. Bésénelle. Grain-scale experimental investigation of localisation phenomena in sand: a discrete particle tracking approach. *Acta Geotechnica*, 7(1):1–13, 2012.

[And15] E.C. Ando. *Experimental investigation of microstructural changes in deforming granular media using x-ray tomography*. PhD thesis, University of Grenoble, France, <https://tel.archives-ouvertes.fr/tel-0144326>, 2015.

[B99] P. Bésénelle. *Déformation et Rupture dans les Roches Tendues et les Solis Indurés : Comparaison Homogène et Localisation*. PhD thesis, Université de Grenoble, France, <https://tel.archives-ouvertes.fr/tel-00094771>, 1999.

[B01a] P. Bésénelle. Compacting and dilating shear bands in porous rock: Theoretical and experimental conditions. *J. Geophys. Res.*, 106(B7):13435–13442, 2001.

[B01b] P. Bésénelle. Evolution of strain localisation with stress in a sandstone: Brittle and semi-brittle regimes. *Phys. Chem. Earth, Part A*, 26(1):21–106, 2001.

[B12] P. Bésénelle. Localisation des déformations dans l’argilite du Callo-Oxfordien. In *International communication*, 2012.

[BBD+08] M. Bornert, F. Brémond, P. Duomail, J.-C. Dupré, M. Fazzini, M. Grédiat, F. Hild, S. Mistou, J. Multon, J. L. Robert, Y. Surel, P. Vacher, and B. Wattrisse. Assessment of digital image correlation measurement errors: methodology and results. *Expér. Mech.*, 3:353–770, 2008.

[BSF599] B.K. Ray, T.S. Smith, D.P. Fyhrig, and M. Saad. Digital image correlation: three-dimensional strain mapping using x-ray tomography digital volume correlation: three-dimensional strain mapping using x-ray tomography. *Expér. Mech.*, 39(3):217–224, 1999.

[CCM01] R. Chambon, D. Caillerie, and T. Matsushima. Plastic continuum with microstructure, local second gradient theories for geomaterials: localization studies. *Int. J. Solids Struct.*, 38(46):8477–8503, 2001.

[Cou90] F. and F. Cosserat. *Théorie des Corps Déformables*. Hermann, Paris, 1990.

[DCMM96] J. Desres, R. Chambon, M. Mokni, and F. Mazzerolle. Void ratio evolution inside shear bands in triaxial sand specimens studied by computed tomography. *Géotechnique*, 46(3):529–546, 1996.

[2012ALERT] [http://www.alcortech.com/pdf\\_july\\_2012](http://www.alcortech.com/pdf_july_2012)

[JHDH+10] S.A. Hall, M. Bornert, J. Desres, Y. Pannier, N. Lenoir, G. Viggiani, and P. Bésénelle. Discrete and continuous analysis of localised deformation in sand using x-ray pCT and volumetric digital image correlation. *Géotechnique*, 60(5):315–322, 2010.

[JHC00] B. Halimoun and C. Chang. A new true triaxial cell for testing mechanical properties of rock, in order to determine rock strength and deformation. In *Proc. of Int. Symp. Rock Mech. and Engng., Beijing, China, 2005*.

[JPX06] B. Pan, H.-m. Xie, and F.-L. Dai. Performance of sub-pixel registration algorithms in digital image correlation. *Mech. Sci. Technol.*, 17:1615–1621, 2006.

[VS95] I. Vardoulakis and J. Sukem. *Bifurcation Analysis in Geomechanics*. Blackie Academic & Professional, Glasgow, 1995.

[VrRHD] E. Verburg, B. van Riebergen, and R. Huiskes. A three-dimensional digital image correlation technique for strain measurements in microstructures. *J. Biomech.*, 37:1313–1320, 2004.

[Tourn04] T. Tournel. *Des écoulements granulaires en régime stationnaire*. Mémoire, Université de la Sorbonne, Paris, 2004.

[DFO04] D. Fournet, O. Molinari, and G. Viggiani. Mesure géométrique volumétrique pour l’étude de la déformation, de la rupture et de la localisation. In *Annales des Géosciences*, 48:279–311, 2004.

[ZFS04] Z. Zhu, F. Follmer, and M. Sulem. A numerical study of the failure process in granular materials under compression. *Comput. Meth. Appl. Mech. Engrg.*, 191:103–124, 2004.

[ZFS05] Z. Zhu, F. Follmer, and M. Sulem. Numerical simulation of the failure process in granular materials under compression. *Comput. Meth. Appl. Mech. Engrg.*, 192:103–124, 2005.

[ZFS06] Z. Zhu, F. Follmer, and M. Sulem. Numerical simulation of the failure process in granular materials under compression. *Comput. Meth. Appl. Mech. Engrg.*, 193:103–124, 2006.

[ZFS07] Z. Zhu, F. Follmer, and M. Sulem. Numerical simulation of the failure process in granular materials under compression. *Comput. Meth. Appl. Mech. Engrg.*, 194:103–124, 2007.

[ZFS08] Z. Zhu, F. Follmer, and M. Sulem. Numerical simulation of the failure process in granular materials under compression. *Comput. Meth. Appl. Mech. Engrg.*, 195:103–124, 2008.

[ZFS09] Z. Zhu, F. Follmer, and M. Sulem. Numerical simulation of the failure process in granular materials under compression. *Comput. Meth. Appl. Mech. Engrg.*, 196:103–124, 2009.

[ZFS10] Z. Zhu, F. Follmer, and M. Sulem. Numerical simulation of the failure process in granular materials under compression. *Comput. Meth. Appl. Mech. Engrg.*, 197:103–124, 2010.

[ZFS11] Z. Zhu, F. Follmer, and M. Sulem. Numerical simulation of the failure process in granular materials under compression. *Comput. Meth. Appl. Mech. Engrg.*, 198:103–124, 2011.

[ZFS12] Z. Zhu, F. Follmer, and M. Sulem. Numerical simulation of the failure process in granular materials under compression. *Comput. Meth. Appl. Mech. Engrg.*, 199:103–124, 2012.

[ZFS13] Z. Zhu, F. Follmer, and M. Sulem. Numerical simulation of the failure process in granular materials under compression. *Comput. Meth. Appl. Mech. Engrg.*, 200:103–124, 2013.

[ZFS14] Z. Zhu, F. Follmer, and M. Sulem. Numerical simulation of the failure process in granular materials under compression. *Comput. Meth. Appl. Mech. Engrg.*, 201:103–124, 2014.

[ZFS15] Z. Zhu, F. Follmer, and M. Sulem. Numerical simulation of the failure process in granular materials under compression. *Comput. Meth. Appl. Mech. Engrg.*, 202:103–124, 2015.

[ZFS16] Z. Zhu, F. Follmer, and M. Sulem. Numerical simulation of the failure process in granular materials under compression. *Comput. Meth. Appl. Mech. Engrg.*, 203:103–124, 2016.

[ZFS17] Z. Zhu, F. Follmer, and M. Sulem. Numerical simulation of the failure process in granular materials under compression. *Comput. Meth. Appl. Mech. Engrg.*, 204:103–124, 2017.

[ZFS18] Z. Zhu, F. Follmer, and M. Sulem. Numerical simulation of the failure process in granular materials under compression. *Comput. Meth. Appl. Mech. Engrg.*, 205:103–124, 2018.

[ZFS19] Z. Zhu, F. Follmer, and M. Sulem. Numerical simulation of the failure process in granular materials under compression. *Comput. Meth. Appl. Mech. Engrg.*, 206:103–124, 2019.

[ZFS20] Z. Zhu, F. Follmer, and M. Sulem. Numerical simulation of the failure process in granular materials under compression. *Comput. Meth. Appl. Mech. Engrg.*, 207:103–124, 2020.

[ZFS21] Z. Zhu, F. Follmer, and M. Sulem. Numerical simulation of the failure process in granular materials under compression. *Comput. Meth. Appl. Mech. Engrg.*, 208:103–124, 2021.

[ZFS22] Z. Zhu, F. Follmer, and M. Sulem. Numerical simulation of the failure process in granular materials under compression. *Comput. Meth. Appl. Mech. Engrg.*, 209:103–124, 2022.

[ZFS23] Z. Zhu, F. Follmer, and M. Sulem. Numerical simulation of the failure process in granular materials under compression. *Comput. Meth. Appl. Mech. Engrg.*, 210:103–124, 2023.

[ZFS24] Z. Zhu, F. Follmer, and M. Sulem. Numerical simulation of the failure process in granular materials under compression. *Comput. Meth. Appl. Mech. Engrg.*, 211:103–124, 2024.

[ZFS25] Z. Zhu, F. Follmer, and M. Sulem. Numerical simulation of the failure process in granular materials under compression. *Comput. Meth. Appl. Mech. Engrg.*, 212:103–124, 2025.

[ZFS26] Z. Zhu, F. Follmer, and M. Sulem. Numerical simulation of the failure process in granular materials under compression. *Comput. Meth. Appl. Mech. Engrg.*, 213:103–124, 2026.

[ZFS27] Z. Zhu, F. Follmer, and M. Sulem. Numerical simulation of the failure process in granular materials under compression. *Comput. Meth. Appl. Mech. Engrg.*, 214:103–124, 2027.

[ZFS28] Z. Zhu, F. Follmer, and M. Sulem. Numerical simulation of the failure process in granular materials under compression. *Comput. Meth. Appl. Mech. Engrg.*, 215:103–124, 2028.

[ZFS29] Z. Zhu, F. Follmer, and M. Sulem. Numerical simulation of the failure process in granular materials under compression. *Comput. Meth. Appl. Mech. Engrg.*, 216:103–124, 2029.

[ZFS30] Z. Zhu, F. Follmer, and M. Sulem. Numerical simulation of the failure process in granular materials under compression. *Comput. Meth. Appl. Mech. Engrg.*, 217:103–124, 2030.

[ZFS31] Z. Zhu, F. Follmer, and M. Sulem. Numerical simulation of the failure process in granular materials under compression. *Comput. Meth. Appl. Mech. Engrg.*, 218:103–124, 2031.

[ZFS32] Z. Zhu, F. Follmer, and M. Sulem. Numerical simulation of the failure process in granular materials under compression. *Comput. Meth. Appl. Mech. Engrg.*, 219:103–124, 2032.

[ZFS33] Z. Zhu, F. Follmer, and M. Sulem. Numerical simulation of the failure process in granular materials under compression. *Comput. Meth. Appl. Mech. Engrg.*, 220:103–124, 2033.

[ZFS34] Z. Zhu, F. Follmer, and M. Sulem. Numerical simulation of the failure process in granular materials under compression. *Comput. Meth. Appl. Mech. Engrg.*, 221:103–124, 2034.

[ZFS35] Z. Zhu, F. Follmer, and M. Sulem. Numerical simulation of the failure process in granular materials under compression. *Comput. Meth. Appl. Mech. Engrg.*, 222:103–124, 2035.

[ZFS36] Z. Zhu, F. Follmer, and M. Sulem. Numerical simulation of the failure process in granular materials under compression. *Comput. Meth. Appl. Mech. Engrg.*, 223:103–124, 2036.

[ZFS37] Z. Zhu, F. Follmer, and M. Sulem. Numerical simulation of the failure process in granular materials under compression. *Comput. Meth. Appl. Mech. Engrg.*, 224:103–124,

# Outline

- Introduction
  - *in situ* observations
  - impacts of strain localisation
- Experimental investigations: methods
  - *post-mortem* observations
  - multiple (internal) measurements
  - full field measurements
- Experimental results (a few)
  - strain localisation in sands
  - strain localisation in rocks
  - the emergence of strain localisation in geomaterials
- Conclusions

# Introduction

*What is strain localisation ?*

- Strain localization is an important phenomenon for geomaterials that appears almost always when a structure is close to rupture.



*Strain localisation during a plane strain compression in a **clay specimen***  
(Viggiani et al, 2001)

Accelerated  
movies

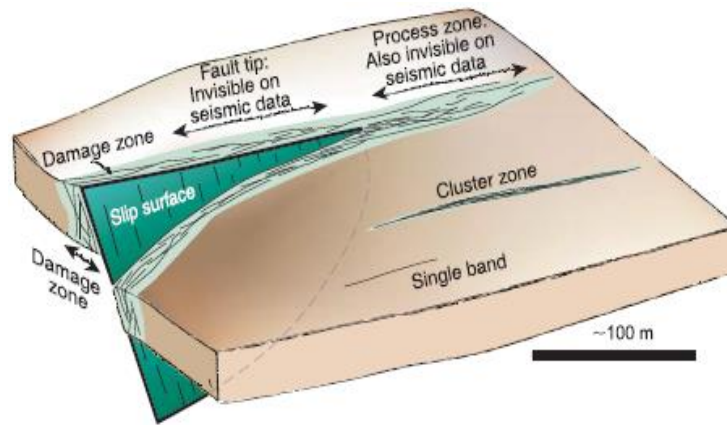


*Strain localisation during a plane strain compression in a **sandstone specimen***  
(Bésuelle et al, 2011)

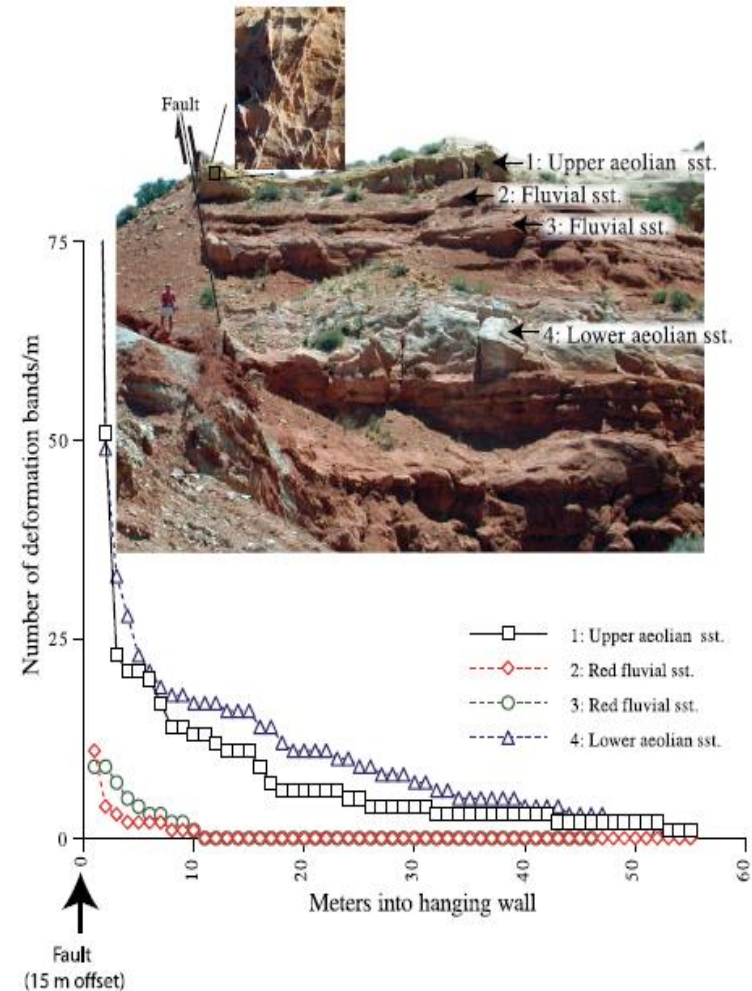


# Introduction

## ➤ *in situ* observations

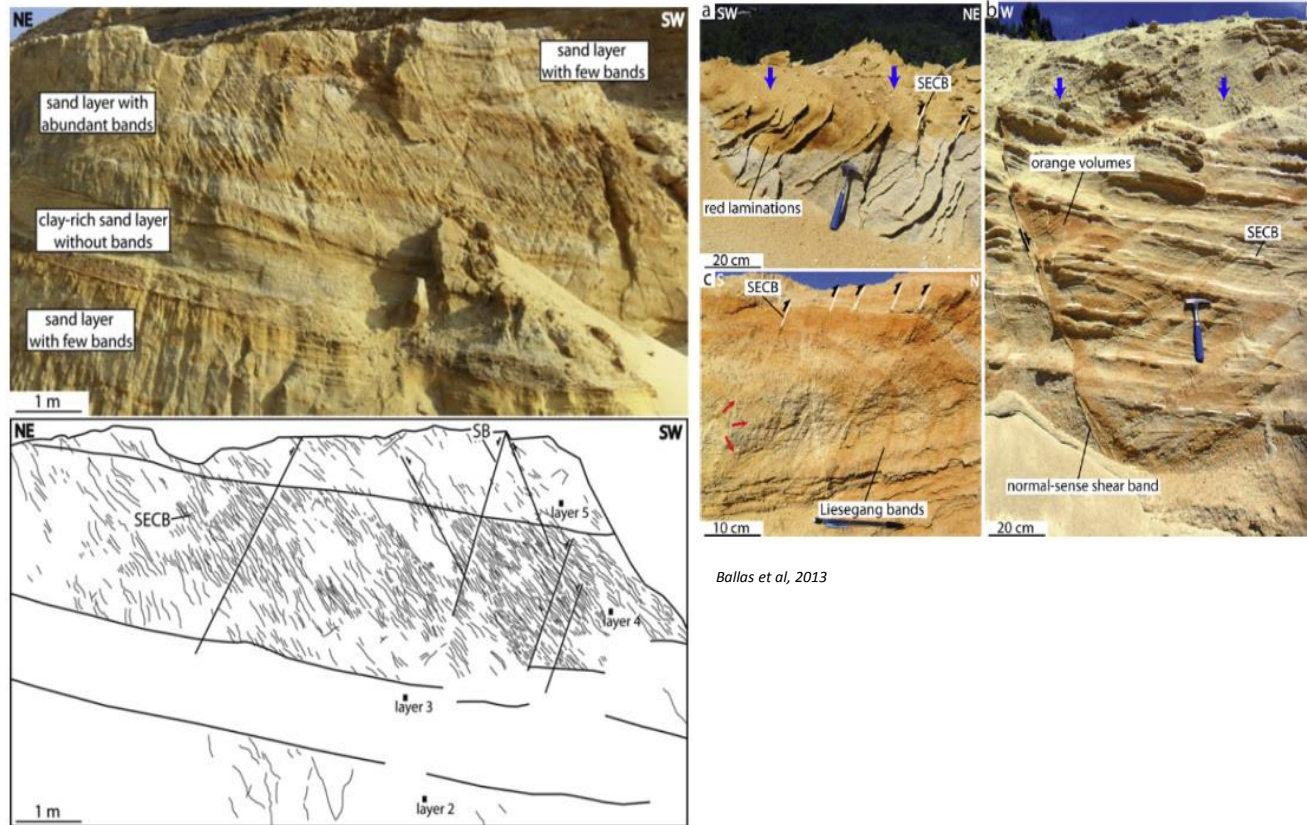


Fossen et al, 2007



# Introduction

## ➤ *in situ* observations



Ballas et al, 2013



# Introduction

➤ *in situ* observations

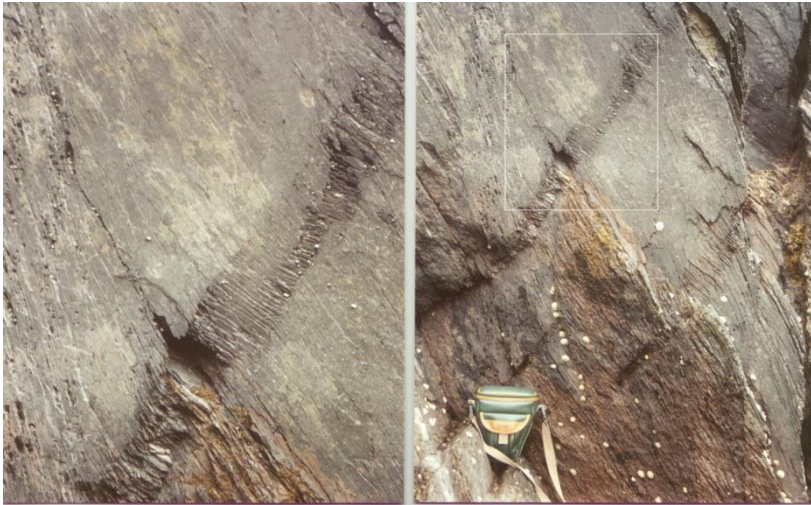


*Courtesy of P. Bésuelle*



# Introduction

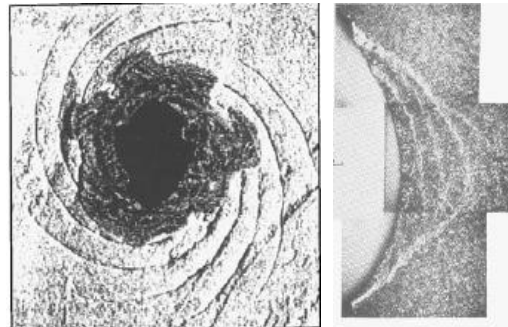
## ➤ *in situ* observations



Courtesy of J. Desrues



Handbook of Materials Behavior (J. Lemaitre ed.) 2001

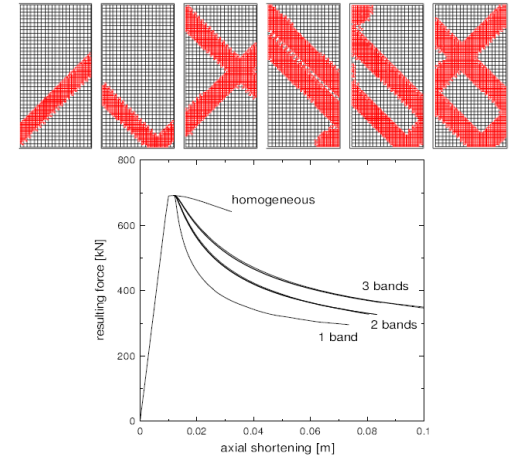


Shear localisation around a galerie



# Introduction

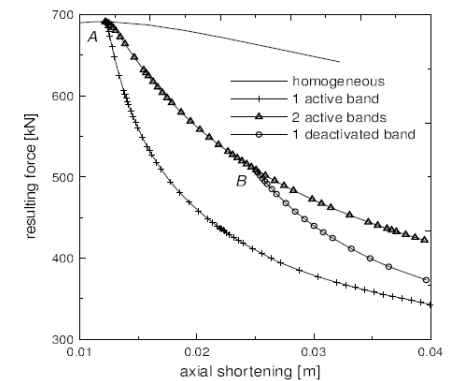
- Some impacts of strain localisation
  - mechanical
    - strain softening
    - damage (elastic properties)
    - mean stress dependency
    - dilatancy/compaction
    - global dispersion of the behaviour
    - hydro mechanical coupling
  - transfer properties
    - permeability change: high permeability channels or impermeable barriers
    - pore geometry change, capillary forces, etc.



*Evidence of post peak dispersion  
(Bésuelle et al, 2006a)*

# Introduction

- Some impacts of strain localisation
  - mechanical
    - strain softening
    - damage (elastic properties)
    - mean stress dependency
    - dilatancy/compaction
    - global dispersion of the behaviour
    - hydro mechanical coupling
  - transfer properties
    - permeability change: high permeability channels or impermeable barriers
    - pore geometry change, capillary forces, etc.

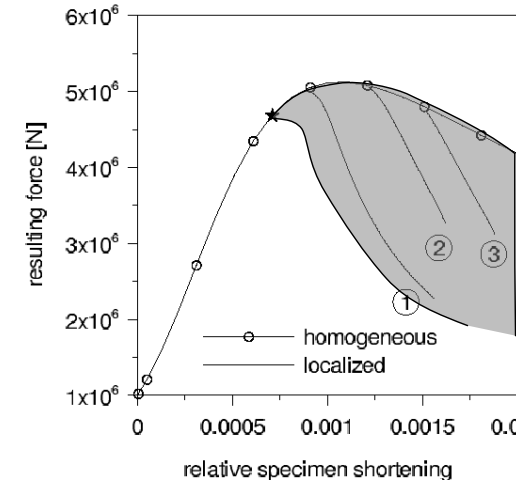


*Evidence of post peak dispersion  
(Bésuelle et al, 2006a)*



# Introduction

- Some impacts of strain localisation
  - mechanical
    - strain softening
    - damage (elastic properties)
    - mean stress dependency
    - dilatancy/compaction
    - global dispersion of the behaviour
    - hydro mechanical coupling
  - transfer properties
    - permeability change: high permeability channels or impermeable barriers
    - pore geometry change, capillary forces, etc.



*Evidence of post peak dispersion  
(Bésuelle et al, 2006b)*

# Introduction

- Some impacts of strain localisation
  - mechanical
    - strain softening
    - damage (elastic properties)
    - mean stress dependency
    - dilatancy/compaction
    - global dispersion of the behaviour
    - hydro mechanical coupling
  - transfer properties
    - permeability change: high permeability channels or impermeable barriers
    - pore geometry change, capillary forces, etc.

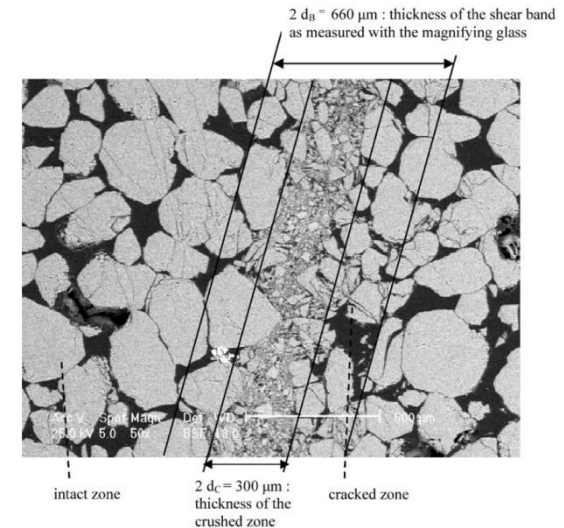


*Evidence of fluid flow channels*



# Introduction

- Some impacts of strain localisation
  - mechanical
    - strain softening
    - damage (elastic properties)
    - mean stress dependency
    - dilatancy/compaction
    - global dispersion of the behaviour
    - hydro mechanical coupling
  - transfer properties
    - permeability change: high permeability channels or impermeable barriers
    - pore geometry change, capillary forces, etc.



*Evidence of grain comminution  
(El Bied et al, 2002)*

# Outline

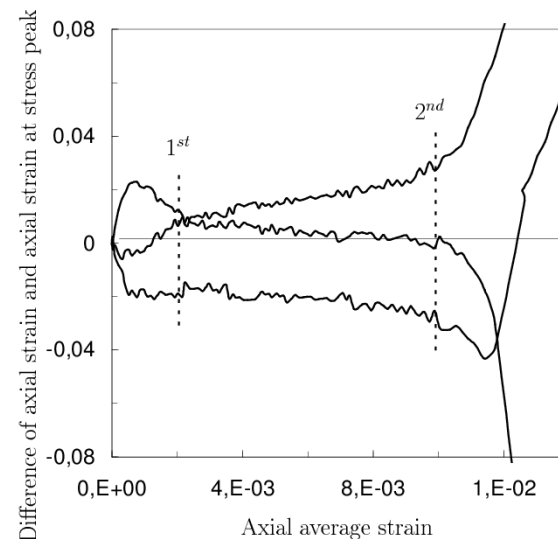
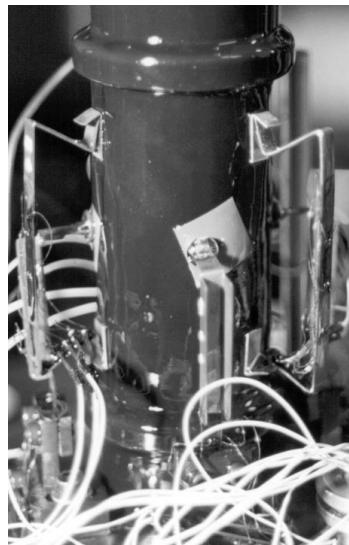
- Introduction
  - *in situ* observations
  - impacts of strain localisation
- Experimental investigations: methods
  - *post-mortem* observations
  - multiple (internal) measurements
  - full field measurements
- Experimental results (a few)
  - strain localisation in sands
  - strain localisation in rocks
  - the emergence of strain localisation in geomaterials
- Conclusions



# Experimental investigations: methods

- *post-mortem* observations
  - strain localisation pattern, etc.
  - microstructural observations
- **detection of strain localisation by multiple internal measurements**
- full field measurements (field quantification + time evolution)
  - non-destructive image tools (tomography)
  - measurement of the kinematic fields (2D + t) or (3D + t)
  - location of acoustic events

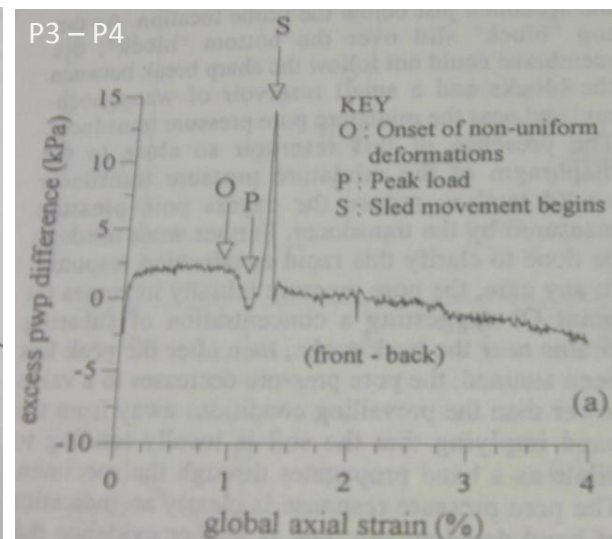
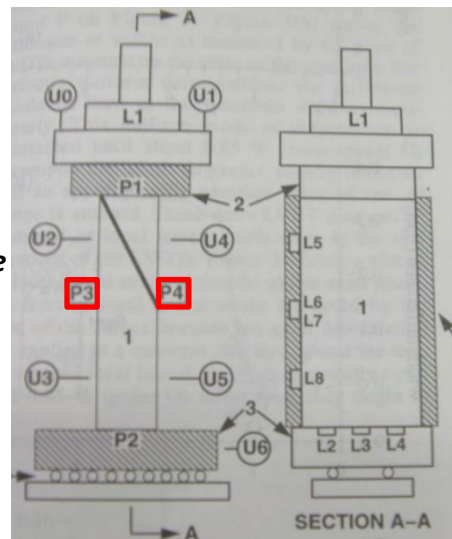
*Detection of the loss of homogeneous deformation with several internal **displacement** transducers*  
(Bésuelle and Desrues, 2001)



# Experimental investigations: methods

- *post-mortem* observations
  - strain localisation pattern, etc.
  - microstructural observations
- **detection of strain localisation by multiple internal measurements**
- full field measurements (field quantification + time evolution)
  - non-destructive image tools (tomography)
  - measurement of the kinematic fields (2D + t) or (3D + t)
  - location of acoustic events

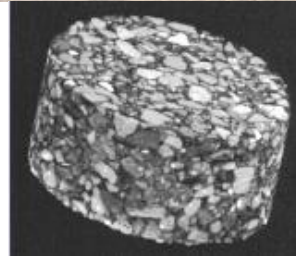
*Evidence of pore pressure gradient induced by strain localisation, observed by several internal **pressure** probes (Viggiani et al, 1994)*





# Experimental investigations: methods

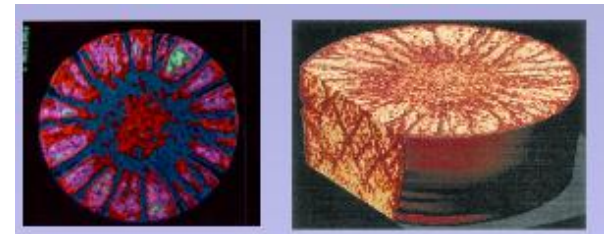
- *post-mortem* observations
  - strain localisation pattern, etc.
  - microstructural observations
- detection of strain localisation by multiple internal measurements
- **full field measurements (field quantification + time evolution)**
  - **non-destructive image tools (tomography)**
  - measurement of the kinematic fields (2D + t) or (3D + t)
  - location of acoustic events



3D picture of a sand specimen  
by **high resolution** X-ray CT  
(3SR Lab)

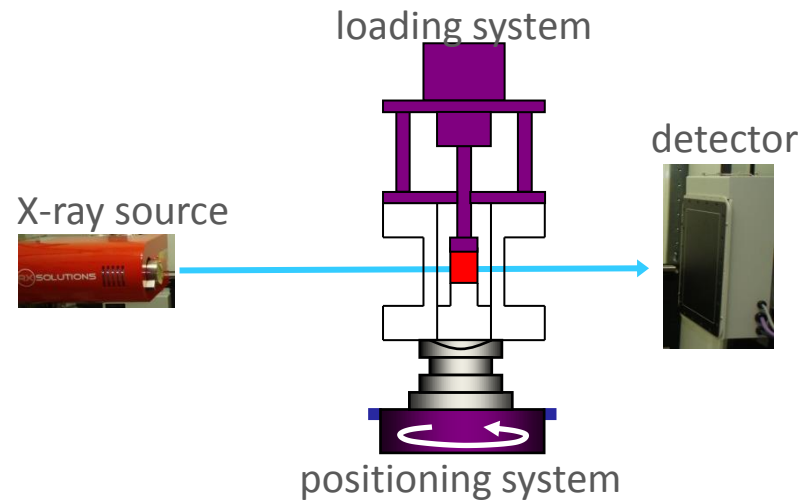
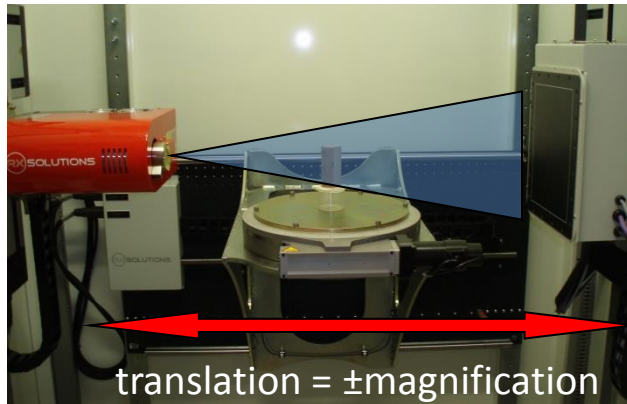


**Low resolution** X-ray CT of sand  
specimens: dilatant bands without grain-  
scale detail (e.g., Desrues et al. [1996];  
Alshibli et al. [2000])



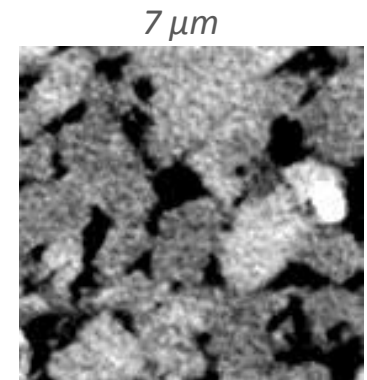
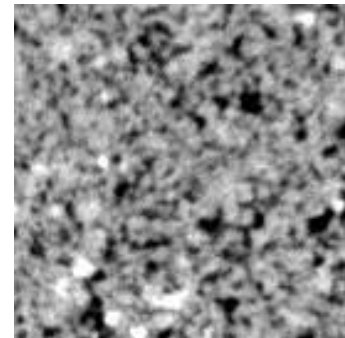
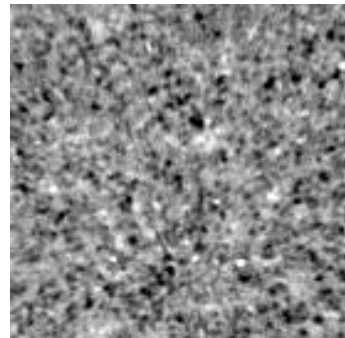
# Experimental investigations: X-ray tomography (CT)

- Industrial/research scanner (conical beam)
- Synchrotron beamline + tomography



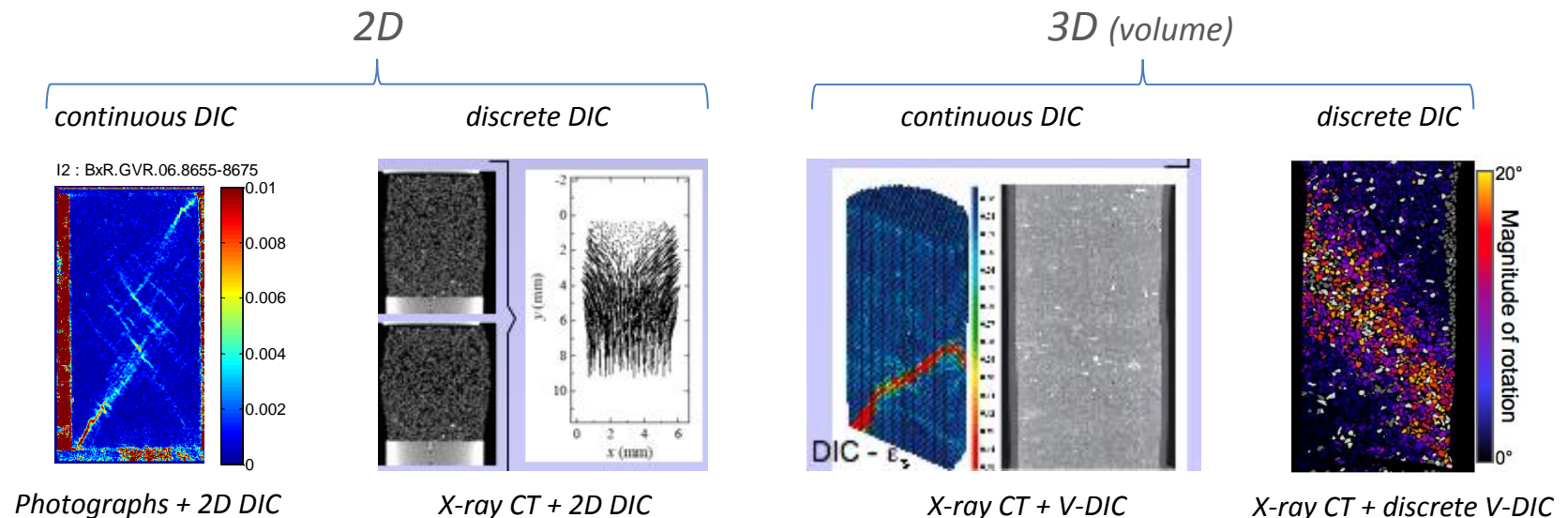
ESRF, Grenoble (France)

Vosges sandstone (grains size  $\sim 300 \mu\text{m}$ )  
voxel width:  $90 \mu\text{m}$



# Experimental investigations: methods

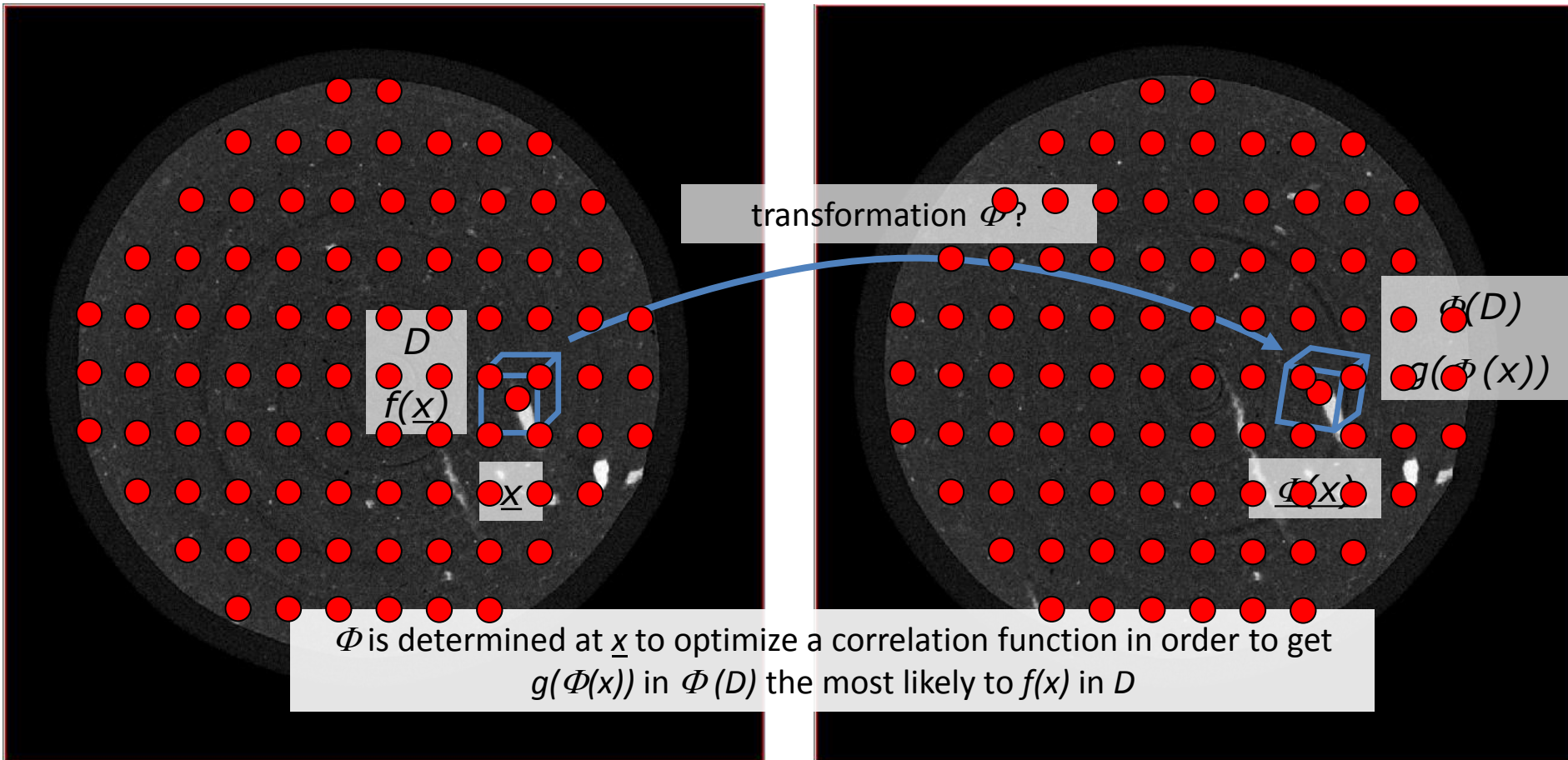
- *post-mortem* observations
  - strain localisation pattern, etc.
  - microstructural observations
- detection of strain localisation by multiple internal measurements
- **full field measurements (field quantification + time evolution)**
  - non-destructive image tools (tomography)
  - **measurement of the kinematic fields (2D + time) or (3D + time)**
  - location of acoustic events





# Experimental investigations: Digital Image Correlation (DIC)

Two 3D-images of the same specimen at two steps of loading (strain increment)



$D$  : subset around the material point

$f(\underline{x})$ : gray level distribution inside  $D$  - *characterizes the material point*

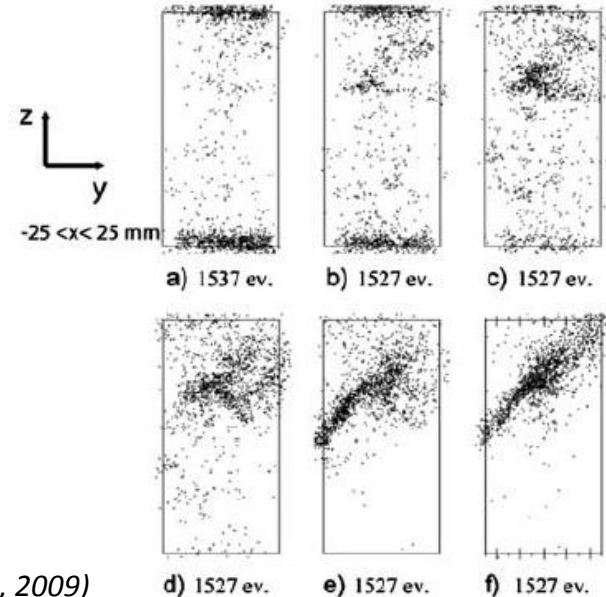
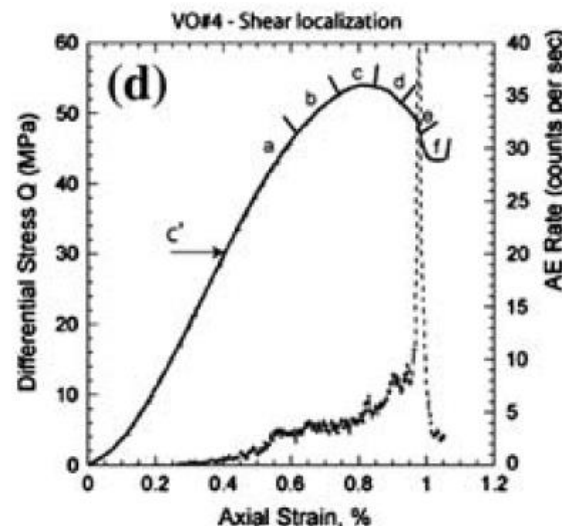
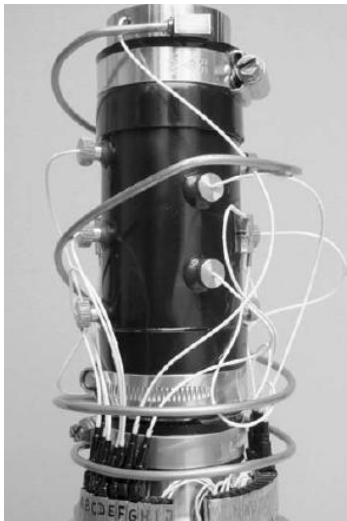
$g(\Phi(\underline{x}))$ : gray level distribution inside  $\Phi(D)$  in the 'deformed' image

# Experimental investigations: Digital Image Correlation

1. The **set of nodes** distributed on the reference image is defined. Generally the nodes are regularly spaced, with a given number of pixels for the distance between nodes.
2. The **subset** around the node is determined, which is generally a square (2D) or a cube (3D) with a size of a few pixels (voxels).
3. The **zone of research** (zone of interest) is determined and the most similar subset in the deformed image is searched.
4. For all possible positions in the research area, a **correlation coefficient** is measured corresponding to a displacement of an integer number of pixels, assuming a rigid displacement (no deformation of the subset). **The position that maximizes the similarity coefficient** is guessed as the best approximation.
5. The previous approximation is refined by a **sub-pixel algorithm**, because the true displacement rarely corresponds to an integer numbers of pixels. Generally, the subset size in this step is smaller than in step **2**. Moreover, the zone of research (step **3**) is reduced to very few pixels (voxels).

# Experimental investigations: methods

- *post-mortem* observations
  - strain localisation pattern, etc.
  - microstructural observations
- detection of strain localisation by multiple internal measurements
- **full field measurements (field quantification + time evolution)**
  - non-destructive image tools (tomography)
  - measurement of the kinematic fields (2D + t) or (3D + t)
  - **location of acoustic events**

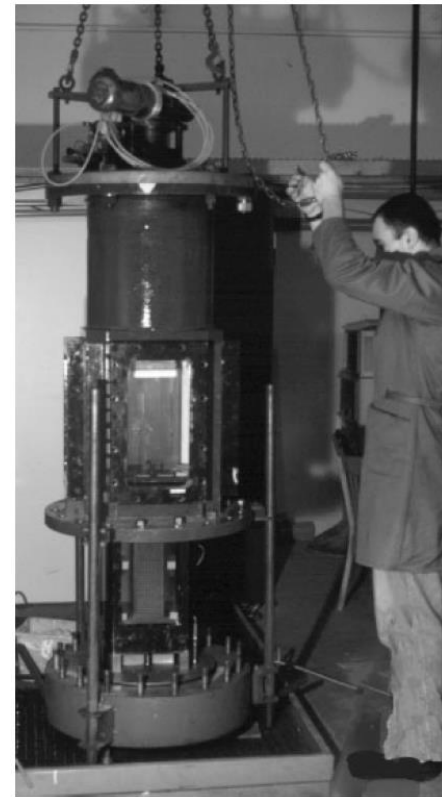
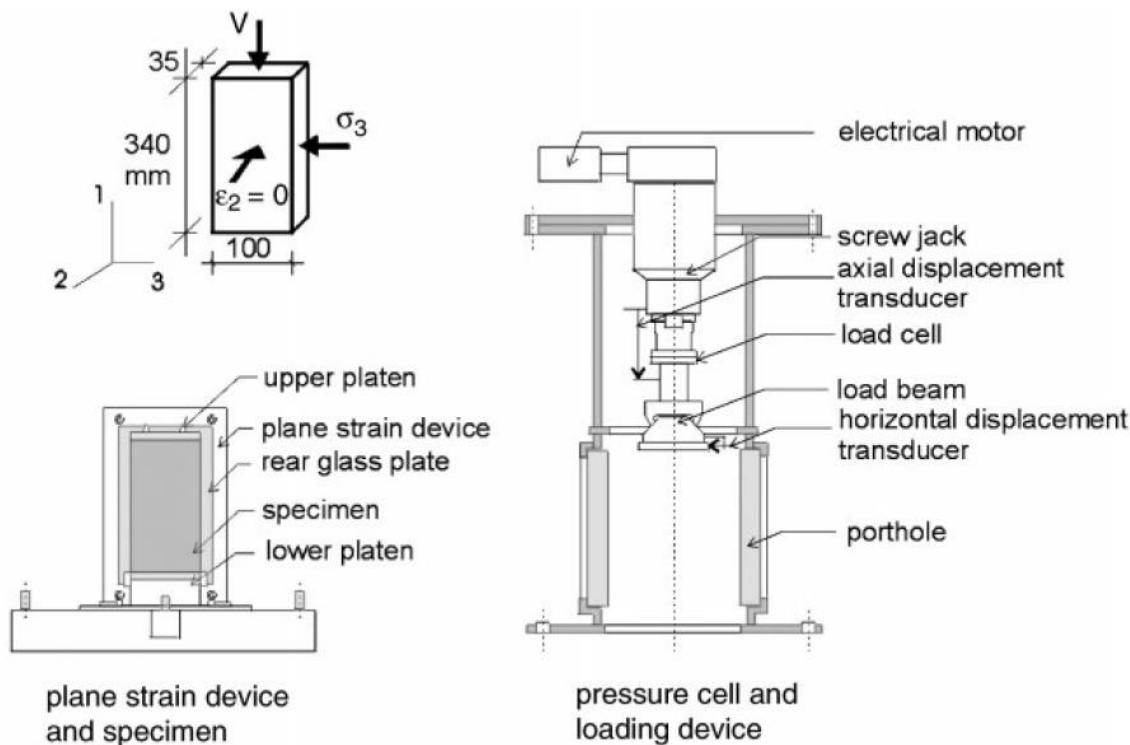


Location of acoustic events during triaxial compression tests (Fortin et al, 2009)



# Experimental investigations: methods

- Cells for full field measurement (need to see the specimen during loading)
  - Plane strain apparatus for soils



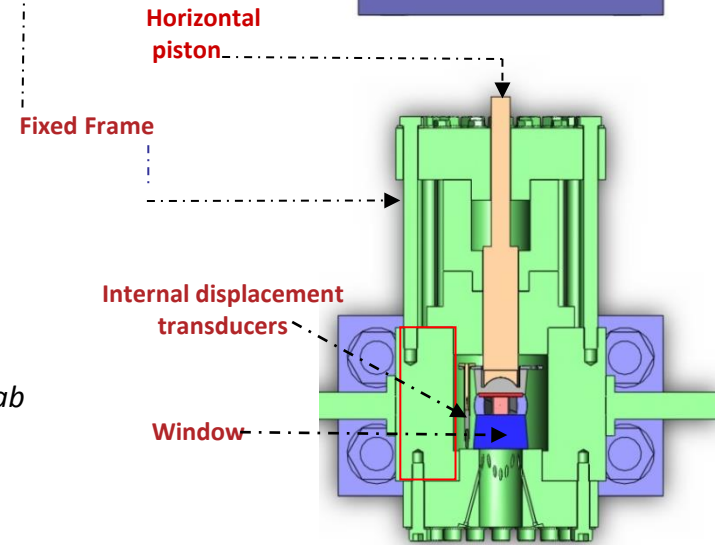
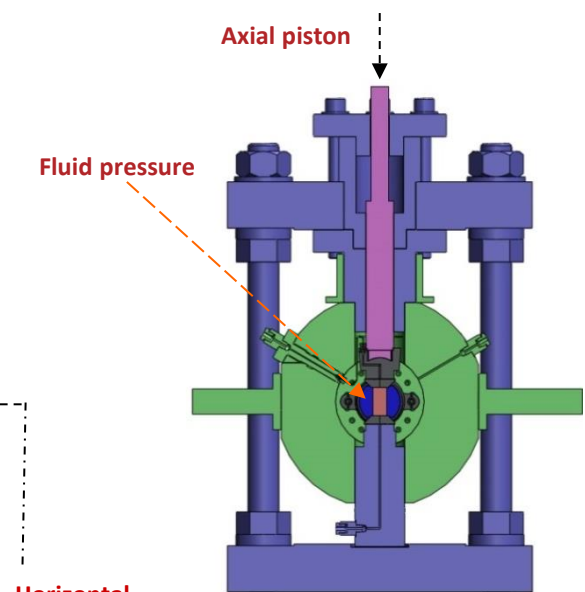
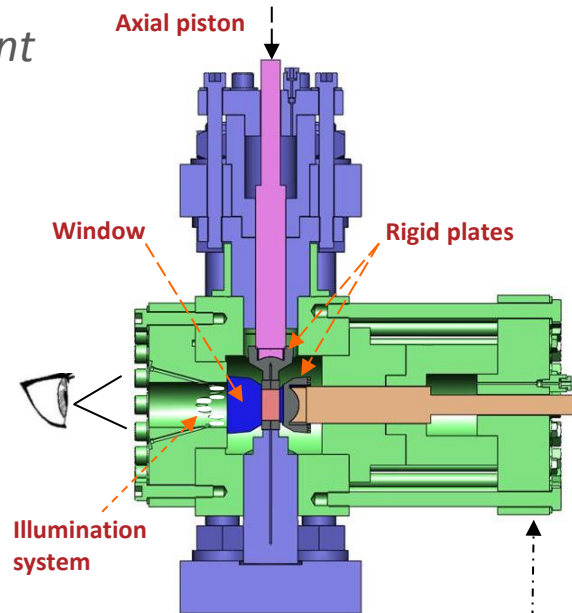
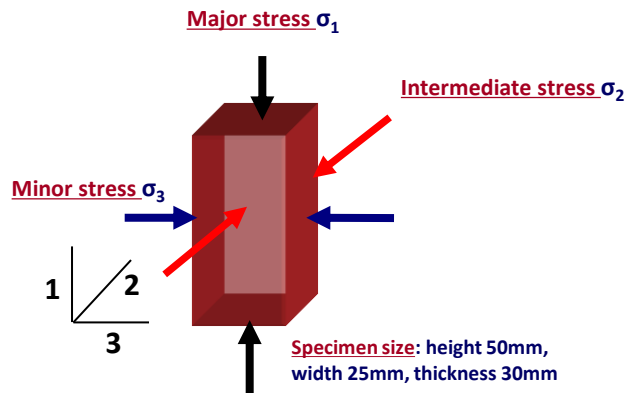
*Plane strain cell at 3SR Lab (Desrues et al)*

# Experimental investigations: methods

## ➤ Cells for full field measurement

### ➤ True triaxial cell for rocks

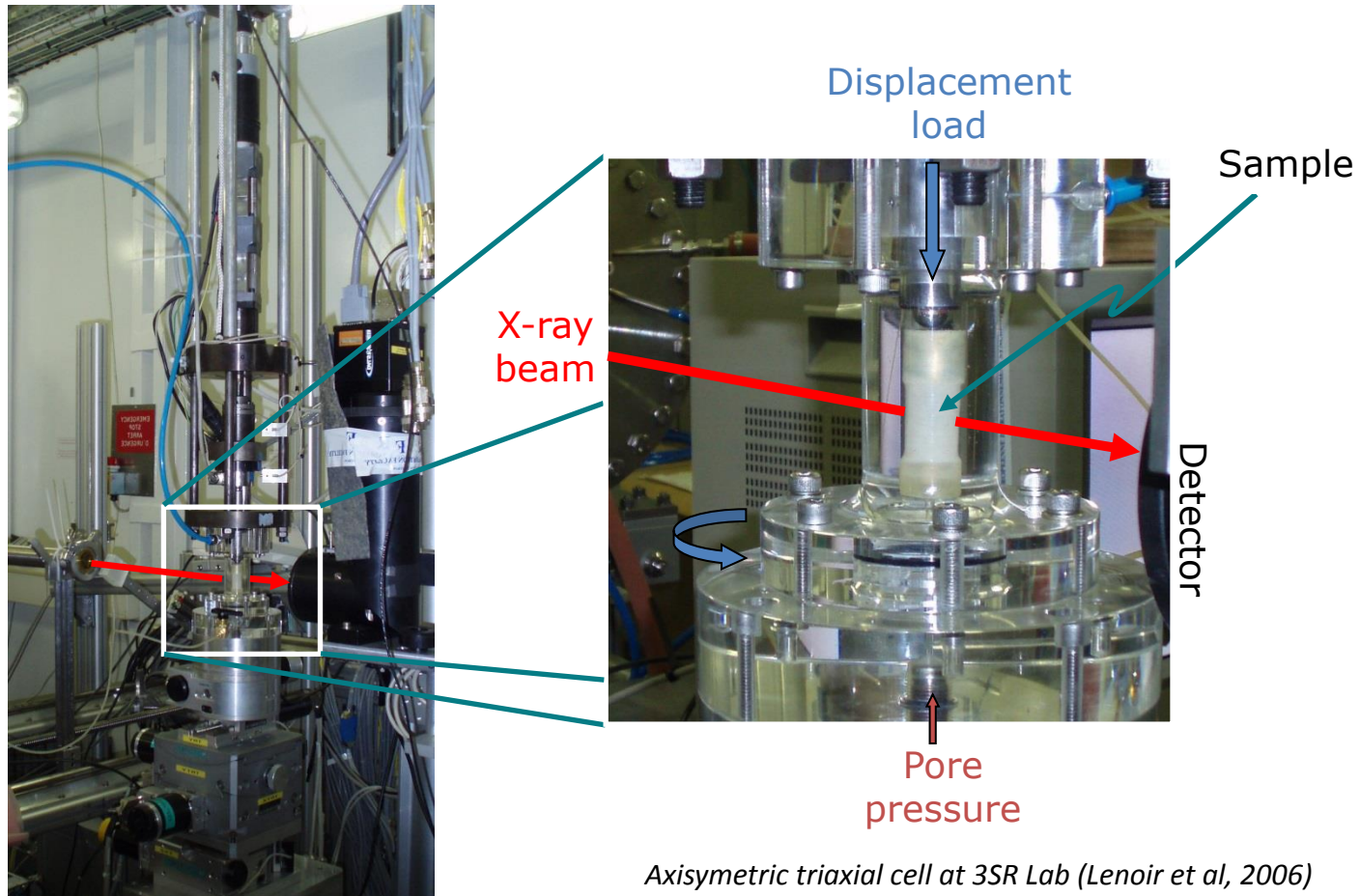
- **Minor stress** : fluid confinement, maxi 100 MPa
- **Intermediate stress** : piston, **force or displacement control**, maxi 650 MPa
- **Major stress** : piston, **force or displacement control**, maxi 750 MPa
- **Window** (sapphire) to see the specimen under loading.



True triaxial cell at 3SR Lab  
(Bésuelle et al, 2016)

# Experimental investigations: methods

- Cells for full field measurement (need to see the specimen during loading)
  - X-ray transparent triaxial cell



Axisymmetric triaxial cell at 3SR Lab (Lenoir et al, 2006)



# Outline

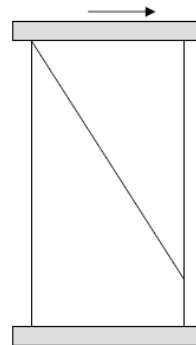
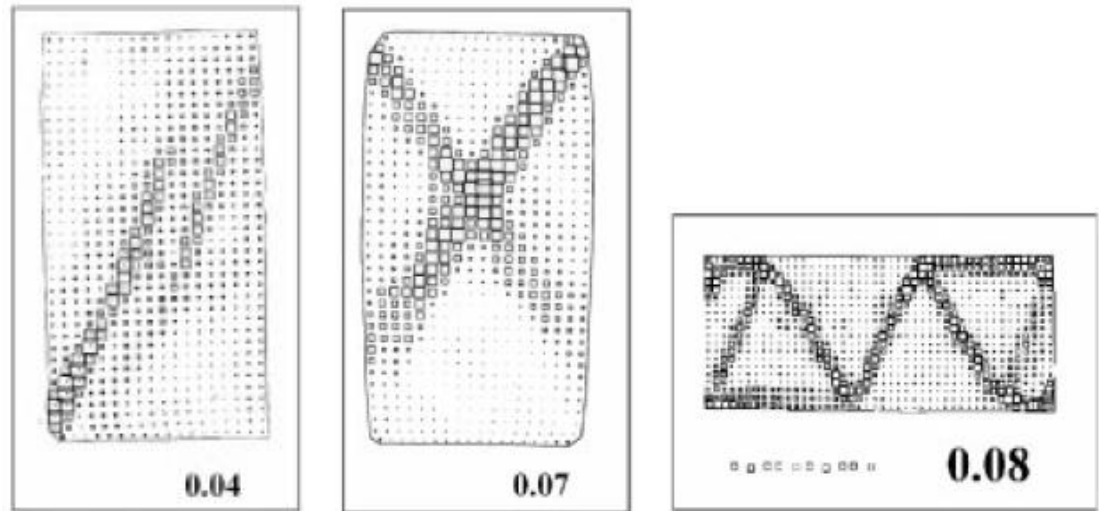
- Introduction
  - *in situ* observations
  - impacts of strain localisation
- Experimental investigations: methods
  - *post-mortem* observations
  - multiple (internal) measurements
  - full field measurements
- **Experimental results (a few)**
  - **strain localisation in sands**
  - strain localisation in rocks
  - the emergence of strain localisation in geomaterials
- Conclusions

# Experimental investigation in sands

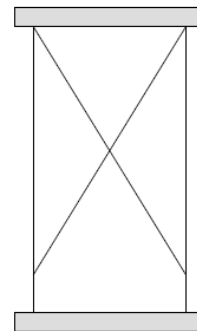
## ➤ Pattern of localisation

*Plane strain compression tests  
(Desrues et al, 1991-2004)*

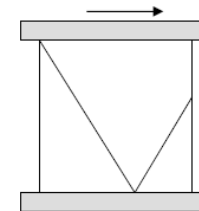
*Effects of the boundaries conditions*



(a)



(b)



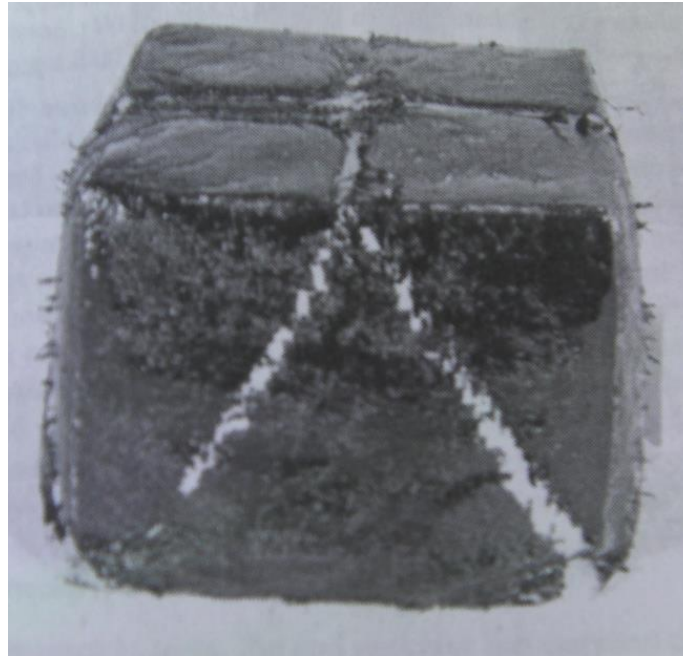
(c)

# Experimental investigation in sands

## ➤ *Pattern of localisation*

*True triaxial compression tests on a cubical specimen (Desrues et al, 1985)*

*Effects of the boundaries conditions:  
Rigid platens on the six specimen's  
surfaces ---> reflexion of shear bands in  
the three spatial directions*

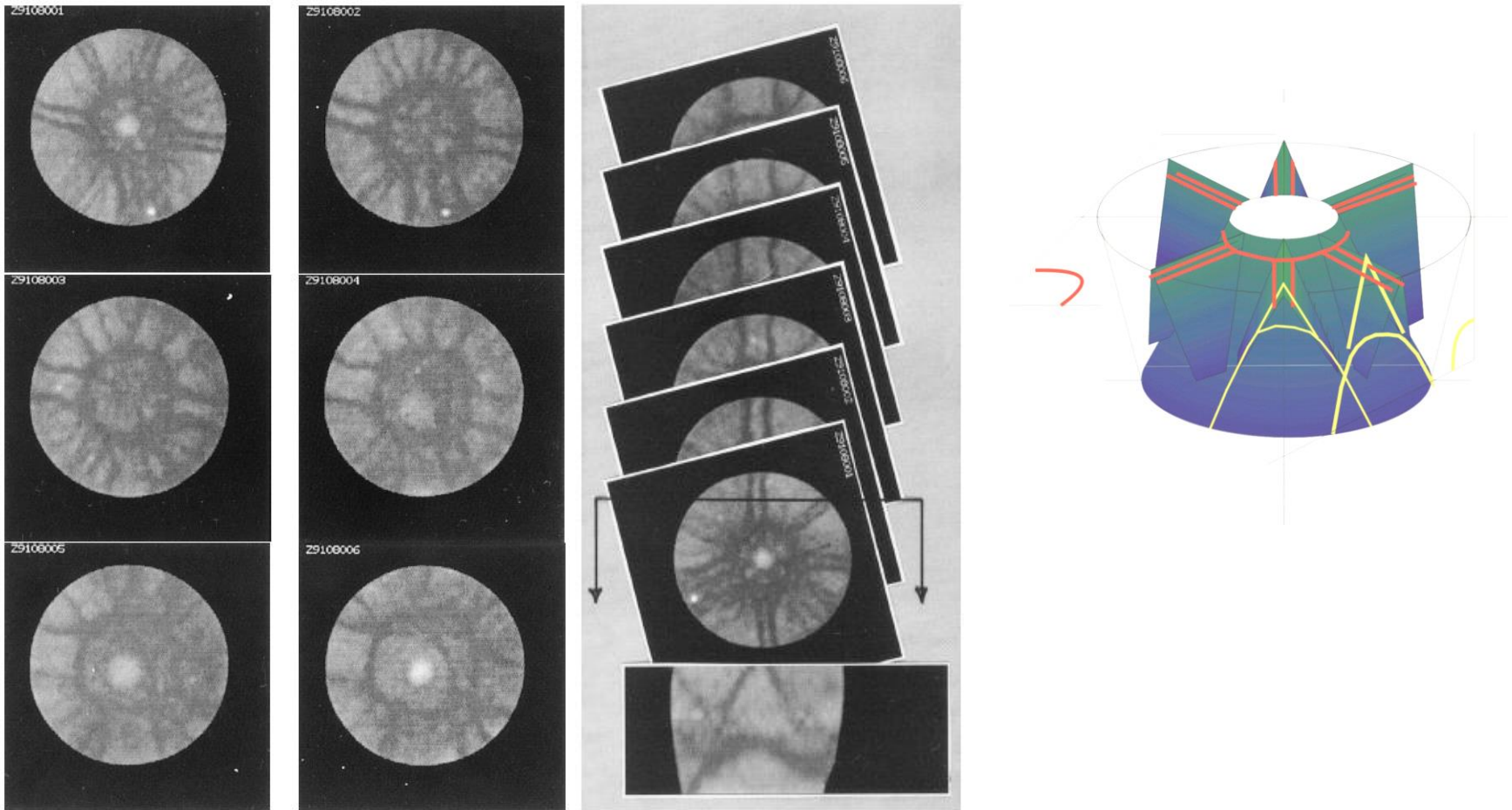




# Experimental investigation in sands

## ➤ Pattern of localisation

*axisymmetric triaxial compression tests (Desrues et al, 1996)*

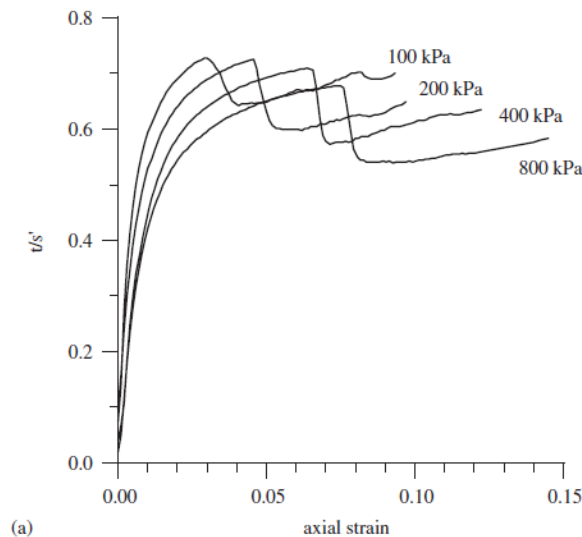


# Experimental investigation in sands

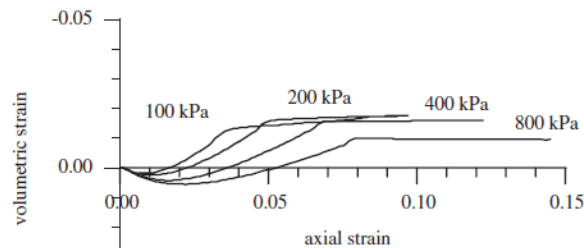
## ➤ Onset of localisation

- Dense and loose specimen
- *Effect of mean stress: Localisation occurs later when mean stress increases*

Dense sand (Desrues et al, 1991-2004)

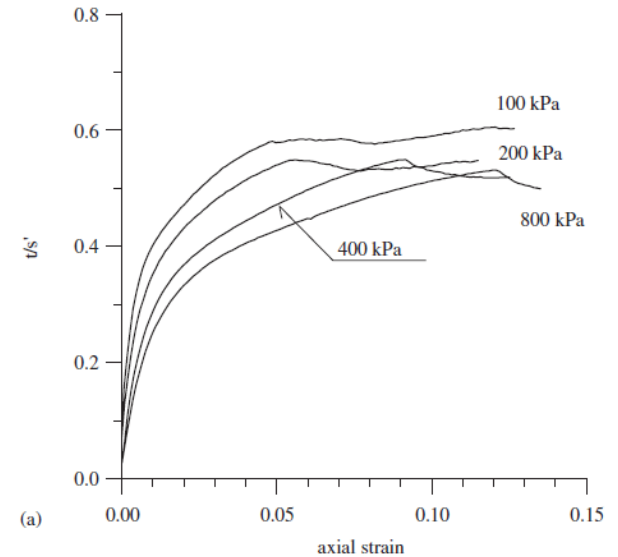


(a)

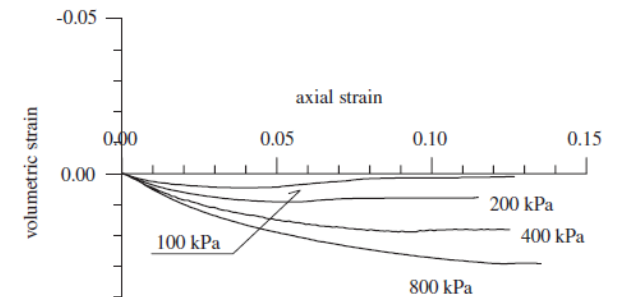


(b)

Loose sand (Desrues et al, 1991-2004)



(a)

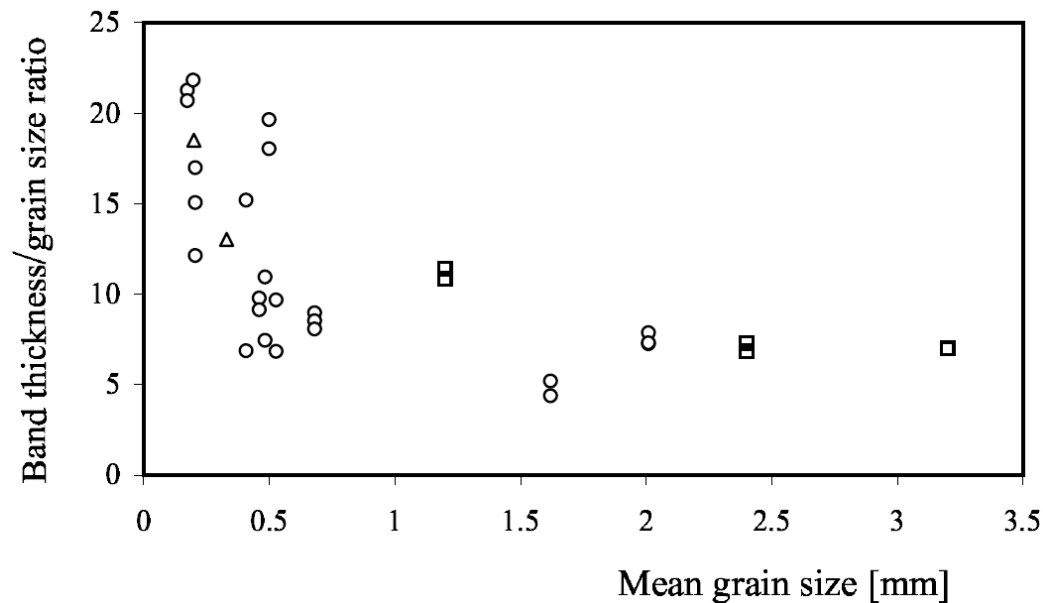


(b)

# Experimental investigation in sands

## ➤ Shear band thickness

*The band thickness is about 5-20 x the mean grain size*



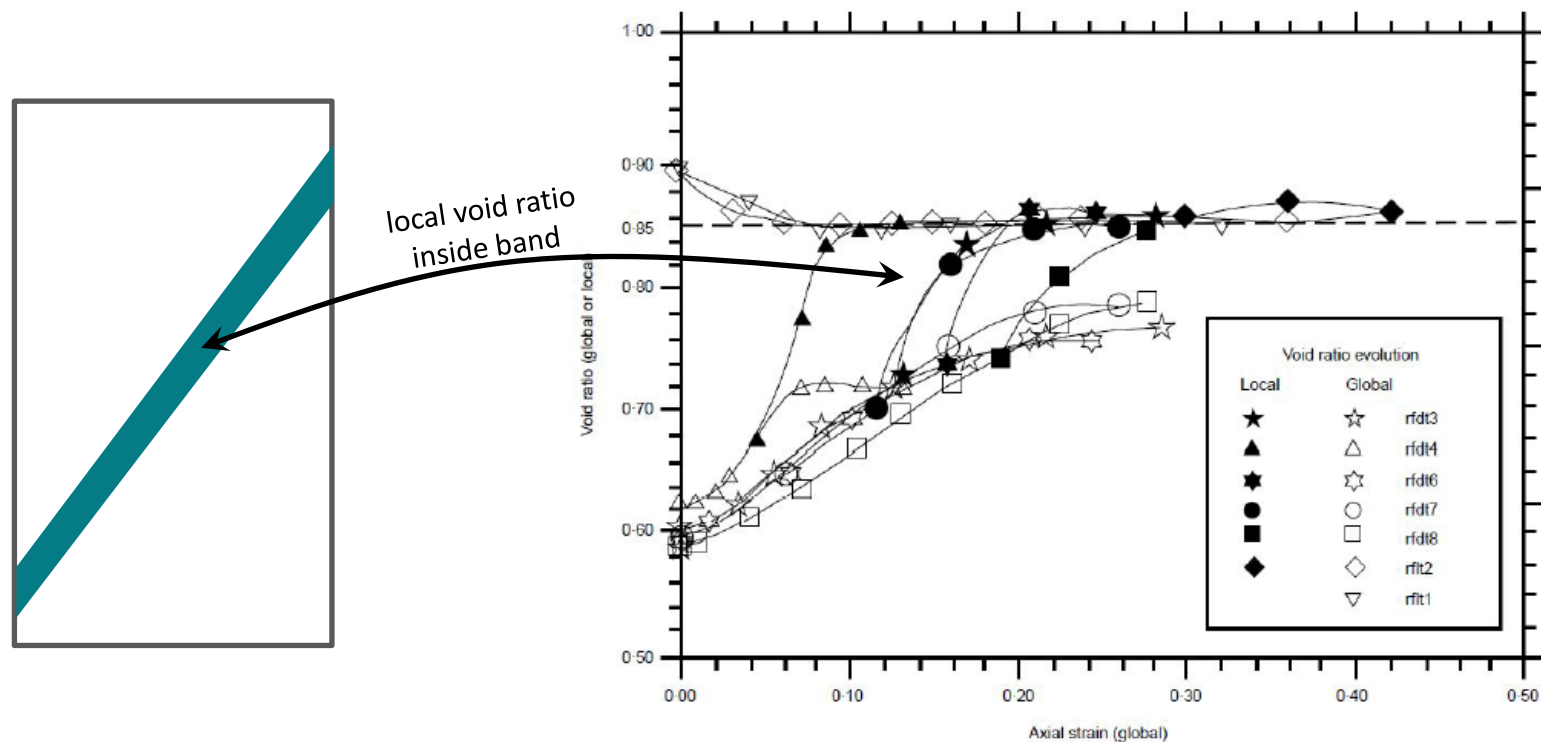
*from Bésuelle and Rudnicki (2006), data from Yoshida and Tatsuoka (1997), Mokni (1992), Mühlhaus and Vardoulakis (1987)*



# Experimental investigation in sands

## ➤ Critical porosity in shear band

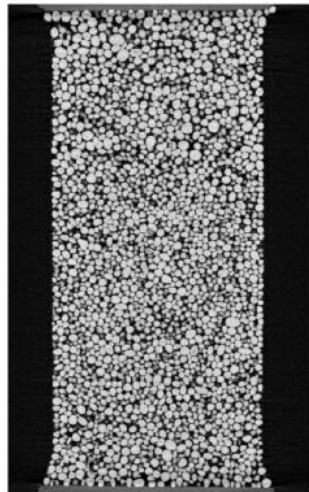
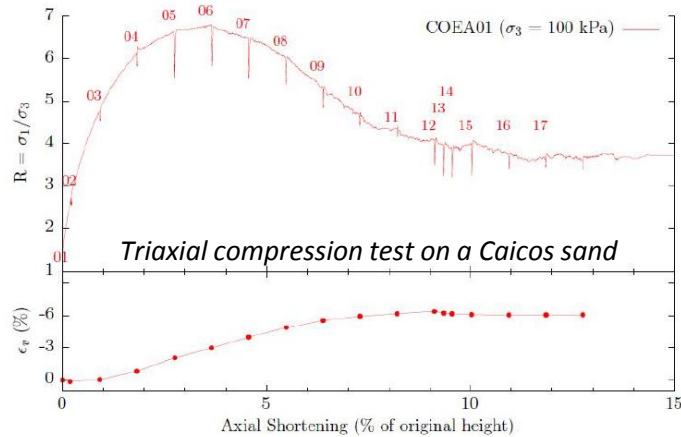
From loose and dense state, the **porosity inside shear bands converges** toward a **critical porosity** (which is mean stress dependant)



from Desrues et al (1996)

# Experimental investigation in sands

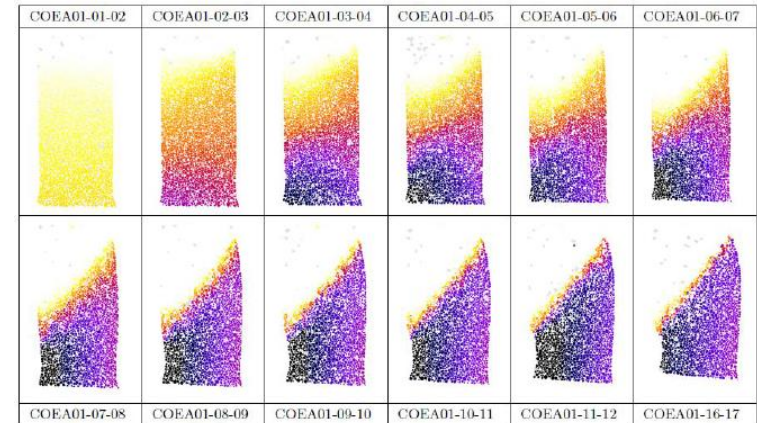
- Grain rearrangement in shear bands: *grains rotation concentration*



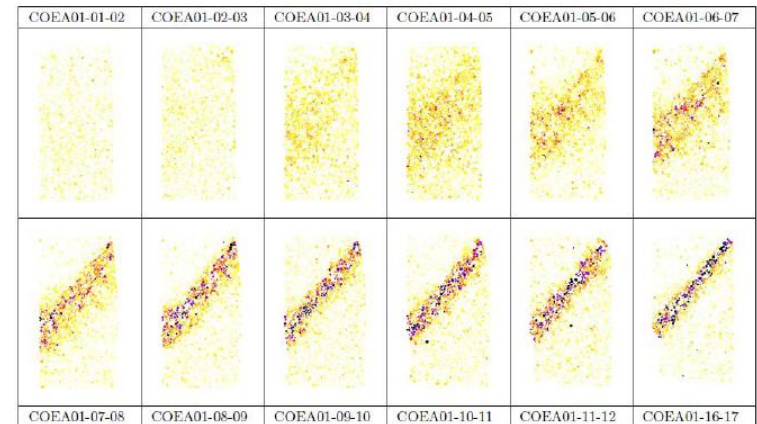
X-ray CT scan  
from Andò (2015)

grains tracking

Rotation angle  
of sand grains



Vertical Displacement  
 $\geq 0$   $\leq -15.4$  px  
 $\leq -239.6$   $\mu\text{m}$  ( $\sim 0.5 D_{50}$ )



Rotation angle  
(axis not shown)  
 $0$   $\geq 20^\circ$

from Andò (2015)

# Outline

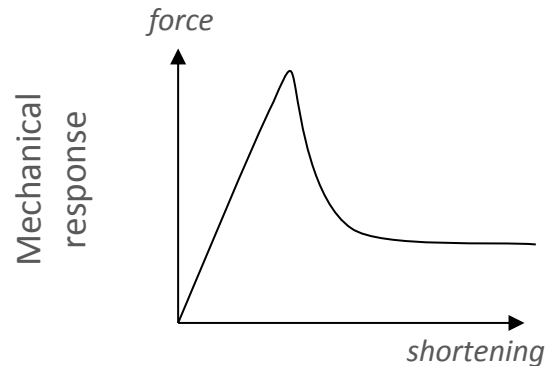
- Introduction
  - *in situ* observations
  - impacts of strain localisation
- Experimental investigations: methods
  - *post-mortem* observations
  - multiple (internal) measurements
  - full field measurements
- **Experimental results (a few)**
  - strain localisation in sands
  - **strain localisation in rocks**
  - the emergence of strain localisation in geomaterials
- Conclusions



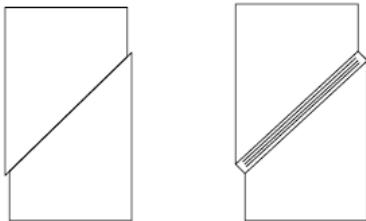
# Experimental investigation in rocks

## ➤ Mechanical responses and failure modes: brittle vs. ductile regimes

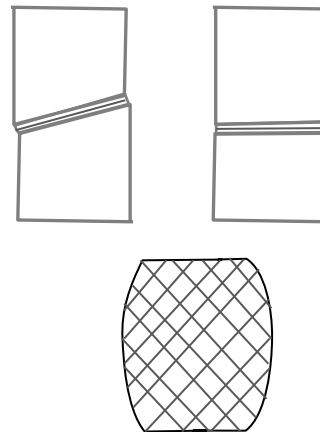
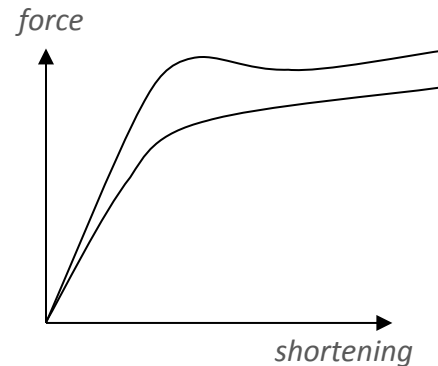
### Brittle



Deformation & failure mode



### Ductile

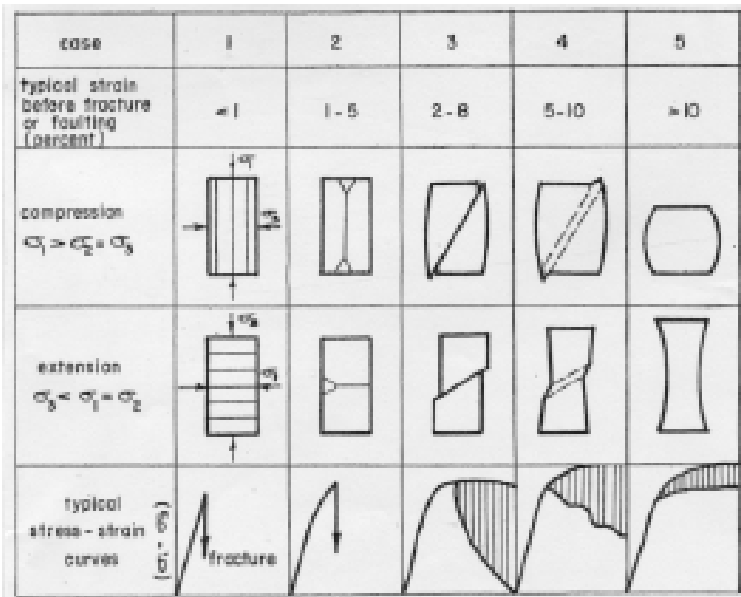


- **Brittle:**
  - a sudden failure, without substantial precursors
  - a strongly localised deformation (fault, shear band)
  - a strong strain softening after the peak
- **Ductile:**
  - able to sustain a substantial deformation
  - a diffuse strain field or highly inclined band
  - no significant stress softening
- **Semi-brittle:** intermediate (localisation without significant stress softening)

**The brittle/ductile failure is not intrinsic to the rock.** A rock can be brittle with a low confining pressure and then ductile with a high confining pressure.

# Experimental investigation in rocks

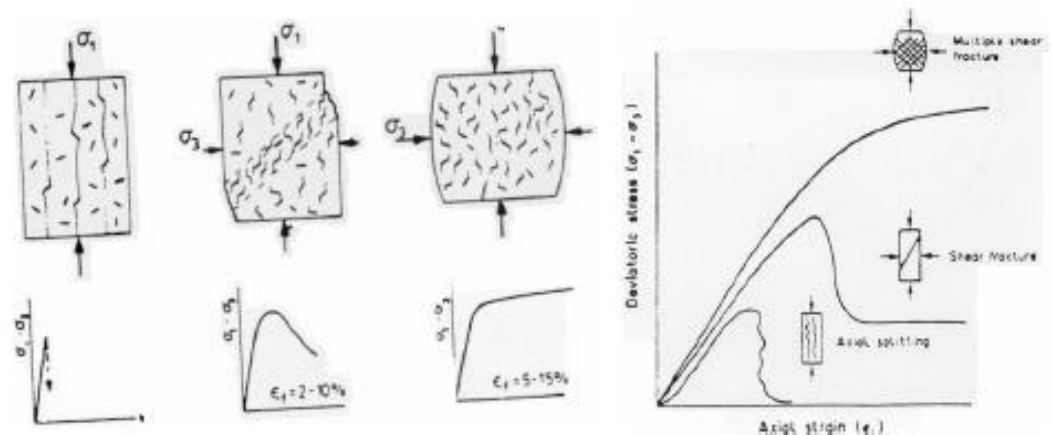
## ➤ Effect of mean stress: failure modes



$\sigma_1$ ,  $\sigma_2$ ,  $\sigma_3$ , are maximum, intermediate, and minimum principal stresses, respectively.

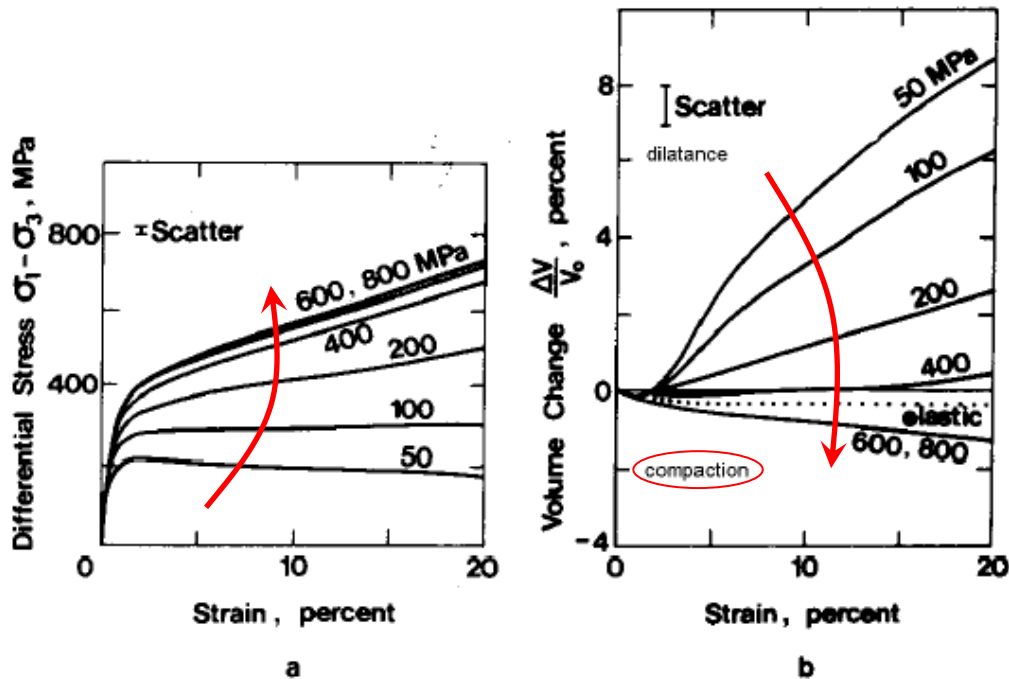
from Paterson (1977)

- No confining pressure: **axial splitting, brittle response**
- 'Medium' confining pressure: **shear band, inclined fracture, strain softening**
- 'Very high' confining pressure: **cataclastic deformation (more or less diffuse) or compaction bands, strain hardening**



# Experimental investigation in rocks

- *Effect of mean stress: mechanical behaviour and failure modes*



A marble

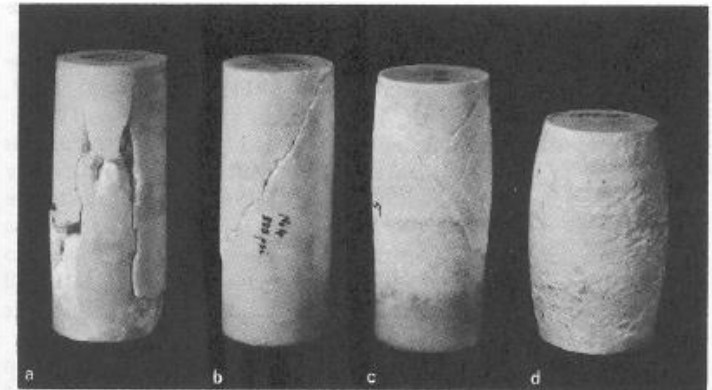


Fig. 48a–d. Types of fractures or flow in Wombeyan marble at various confining pressures: a axial splitting failure at atmospheric pressure; b single shear failure at 3.5 MPa (35 bars); c conjugate shears at 35 MPa (350 bars); d ductile behaviour at 100 MPa (1 kbar). (From experiments of the author; cf. Paterson, 1958)

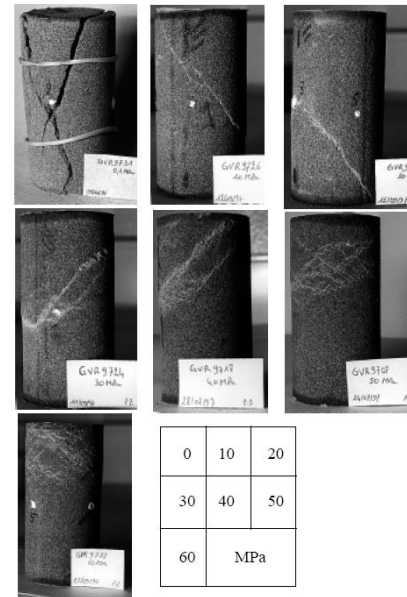
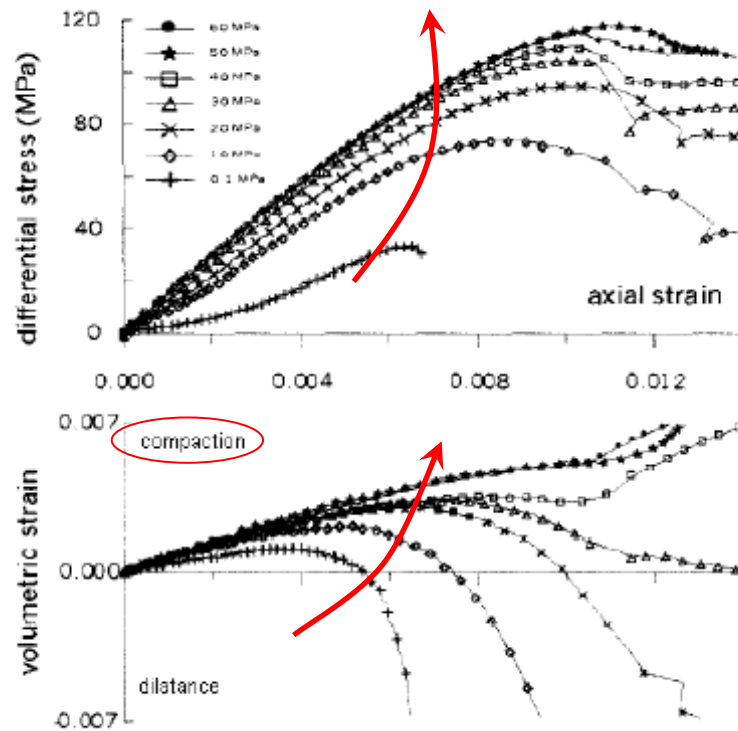
*from Paterson and Wong (2005)*



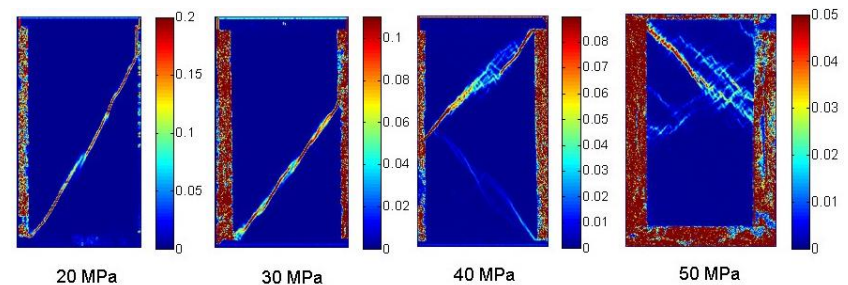
# Experimental investigation in rocks

- *Effect of mean stress: mechanical behaviour and failure modes*

A sandstone



from Bésuelle et al (2000)



Plane strain compression tests, increments of the 2<sup>nd</sup> strain invariant, from Lanatà (2015)

# Experimental investigation in rocks

- *Effect of mean stress: mechanical behaviour and failure modes*

A sandstone

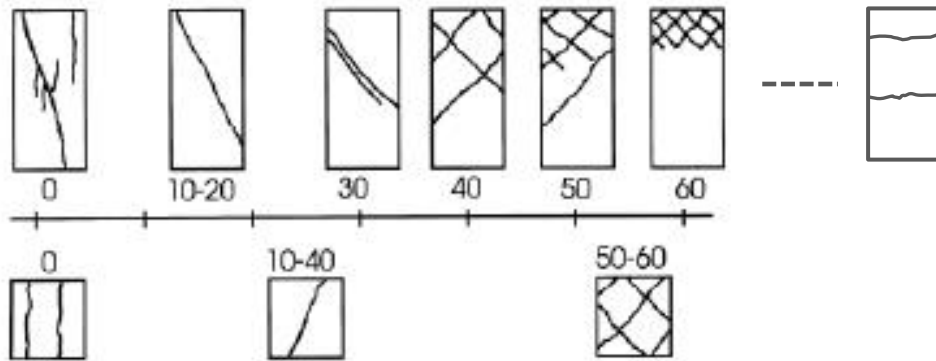


Fig. 6. Observed shear band patterns versus confining pressure for compression test with  $H/D = 2$  and 1. The angle of the bands with respect to the major principal stress increases with the confining pressure, and bands become more and more numerous and close.

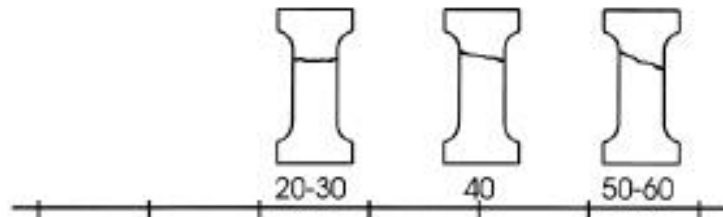
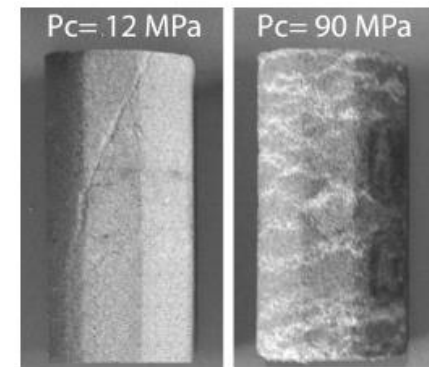


Fig. 9. Observed shear band patterns versus confining pressure for extension test.

from Bésuelle et al (2000)



Shear band & compaction band

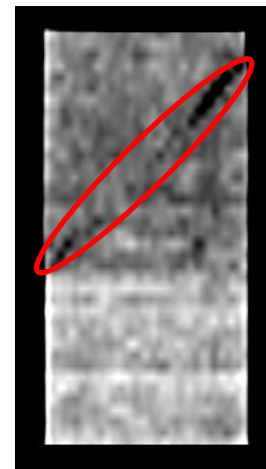
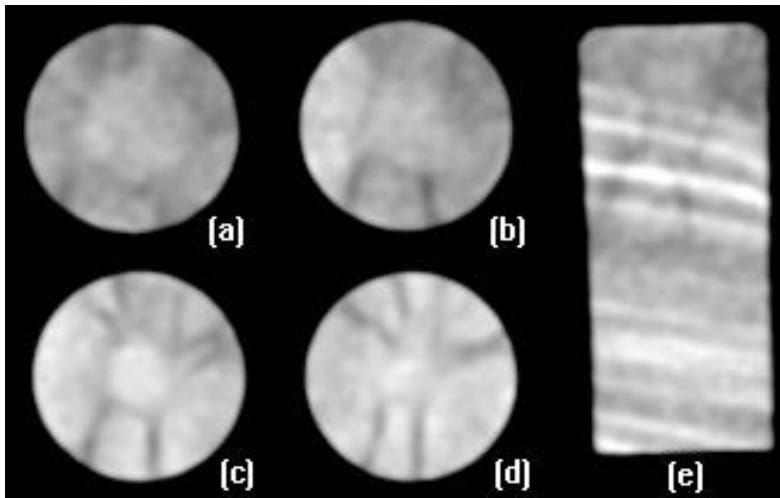


from Fortin et al (2006)

# Experimental investigation in rocks

- *Effect of mean stress: volume strain inside shear bands in porous rocks*

A sandstone

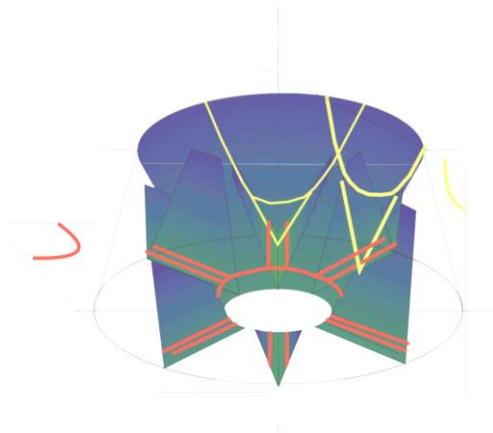


30 MPa  
SB with dilation



50 MPa  
SB with compaction

*from Bésuelle et al (2000)*



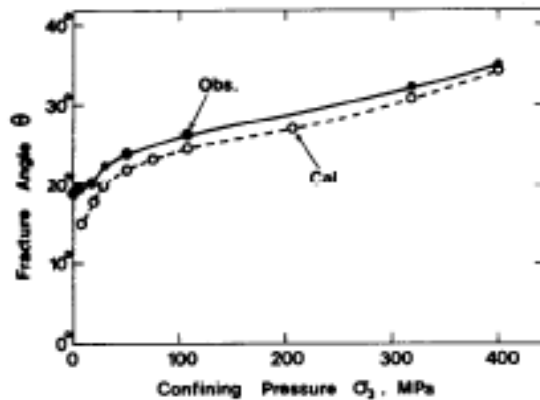
For porous rocks, the volume strain inside shear band is dilative at low mean stress and can be compactive at high mean stress



# Experimental investigation in rocks

## ➤ Effect of mean stress: shear band orientation

Granite



from Mogi et al (1966)

Fig. 10. Relation between confining pressure and inclination  $\theta$  of shear fracture to compression direction in Westerly granite; closed circle: observed angle; open circle: angle calculated from coefficient of internal friction  $\phi$  according to  $\theta = 1/4 \pi - 1/2 \phi$ . (After Mogi, 1966a)

Sandstone

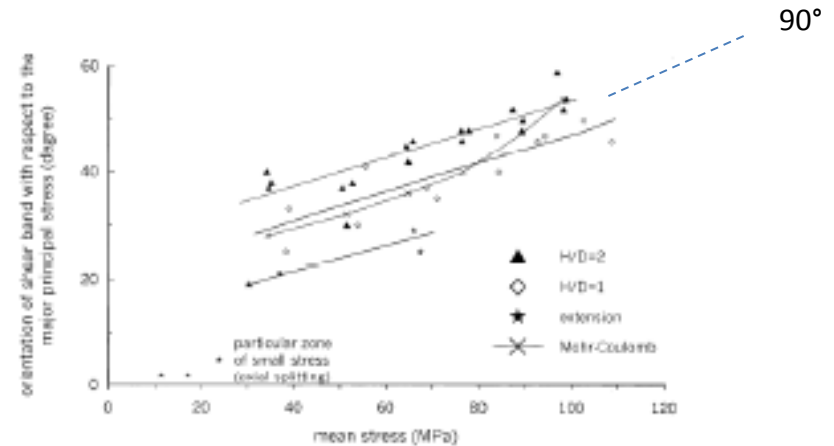


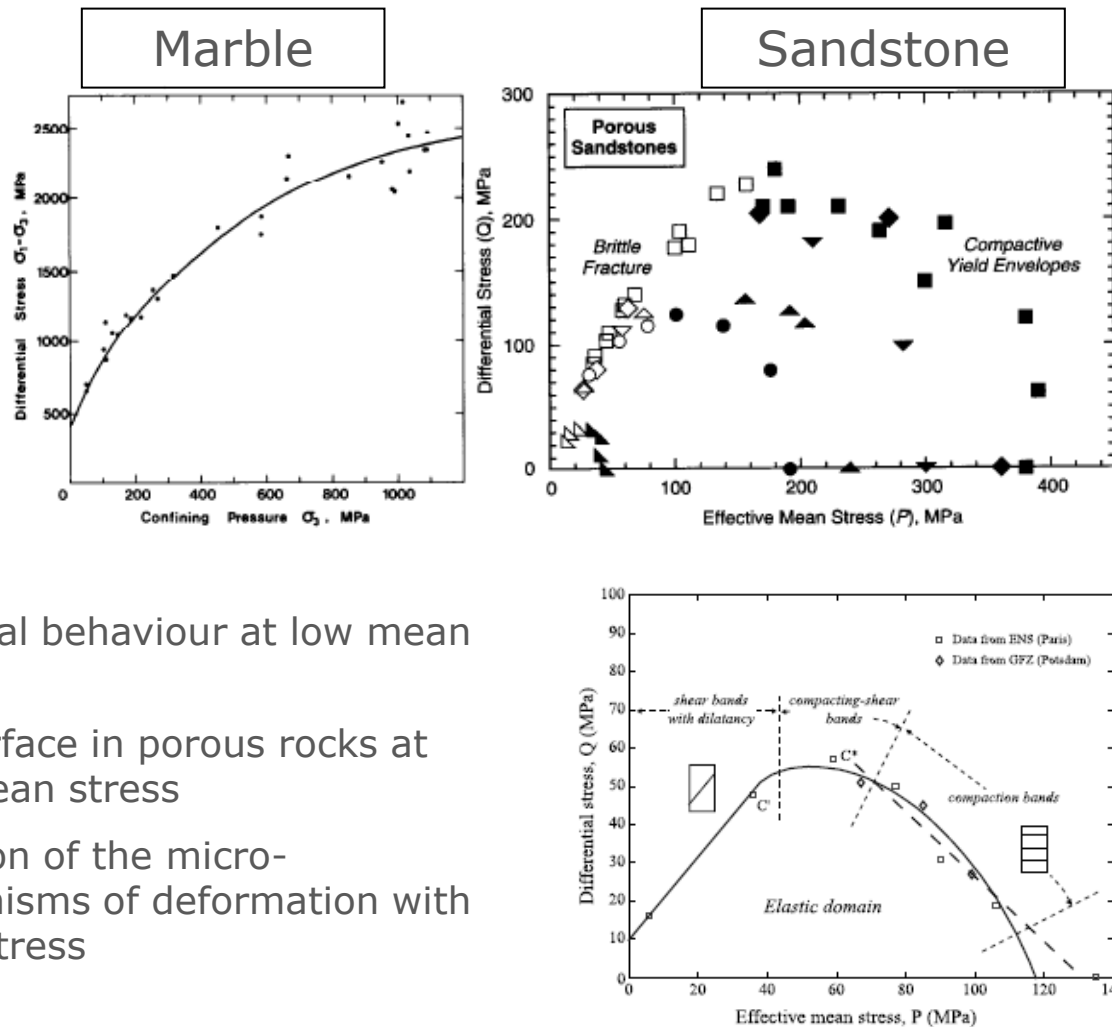
Fig. 8. Orientation of the shear bands with respect to the major principal stress axis versus the mean stress at failure, for compression ( $H/D = 1$  and  $2$ ) and extension test. Solid line shows the prediction with the Mohr-Coulomb criterion:  $\theta = 45^\circ - \phi/2$ , for the  $H/D = 2$  compression tests.

from Bésuelle et al (2000)

The angle between the maximum stress direction and the shear band tends to increase with the mean stress

# Experimental investigation in rocks

## ➤ Effect of mean stress: failure envelope

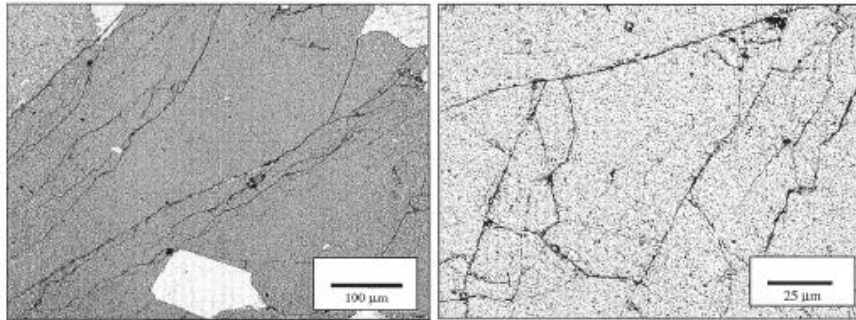


- Frictional behaviour at low mean stress
- Cap surface in porous rocks at high mean stress
- Evolution of the micro-mechanisms of deformation with mean stress

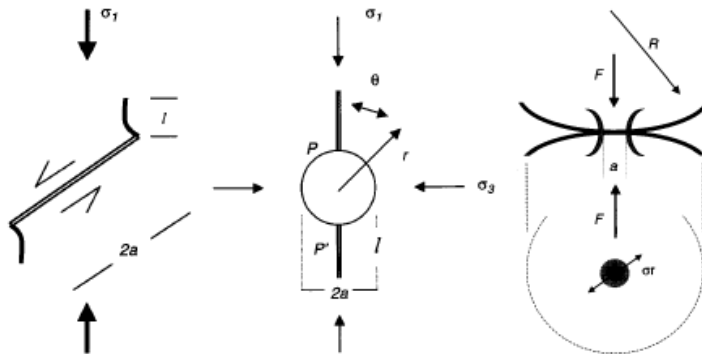
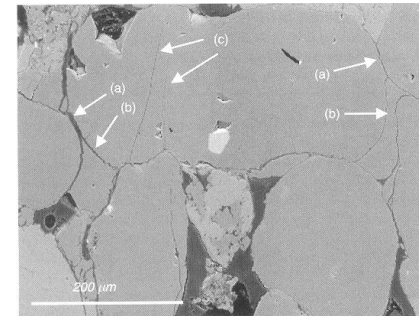
# Experimental investigation in rocks

## ➤ Effect of mean stress: micro-mechanisms of deformation

granite



sandstone



from Guéguen et al (2004)

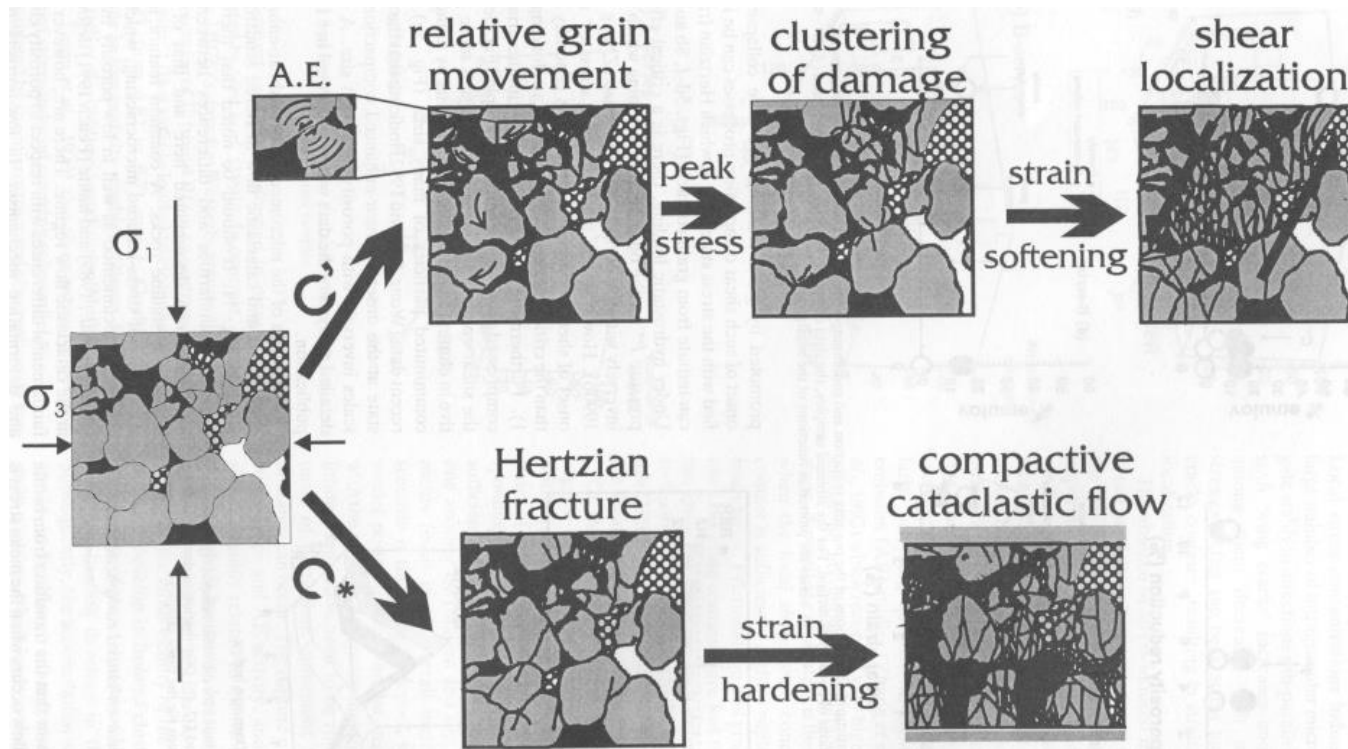
Conceptual crack initiation reasons:

- propagation of a crack from initial fissure (in mode I),
- crack initiation from an (equant) pore (concentration of tensile stress)
- crack initiation at a grain contact (Hertzian fracturation - concentration of tensile stress)



# Experimental investigation in rocks

## ➤ Effect of mean stress: micro-mechanisms of deformation



from Ménendez et al (1996)

- Grain breakage
- Inter and intra granular cracks
- dilatancy

- Grain crushing
- Pore collapse
- compaction

# Experimental investigation in rocks

## ➤ Effect of mean stress: micro-mechanisms of deformation (sandstone)

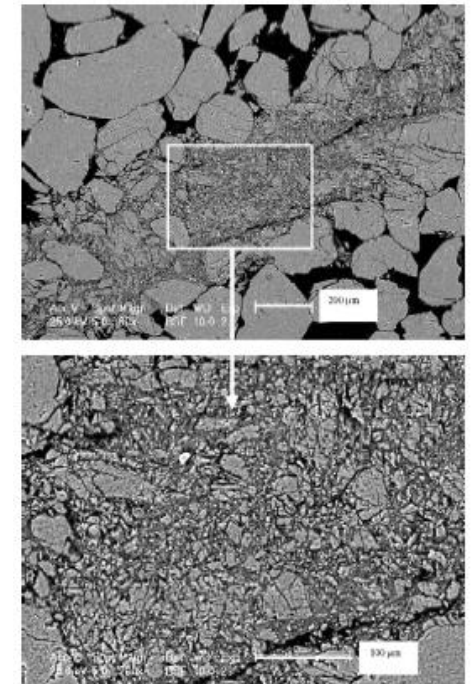
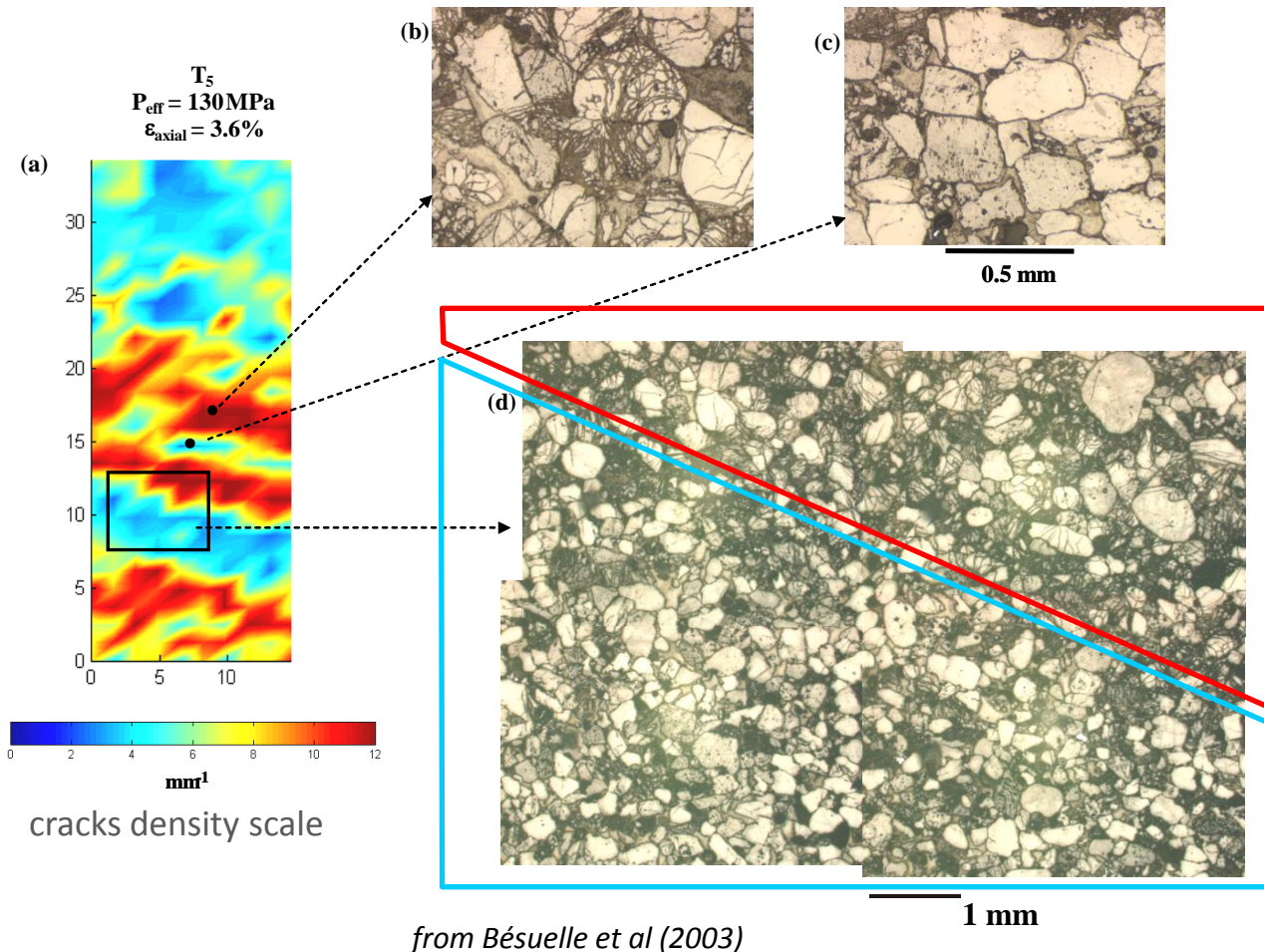
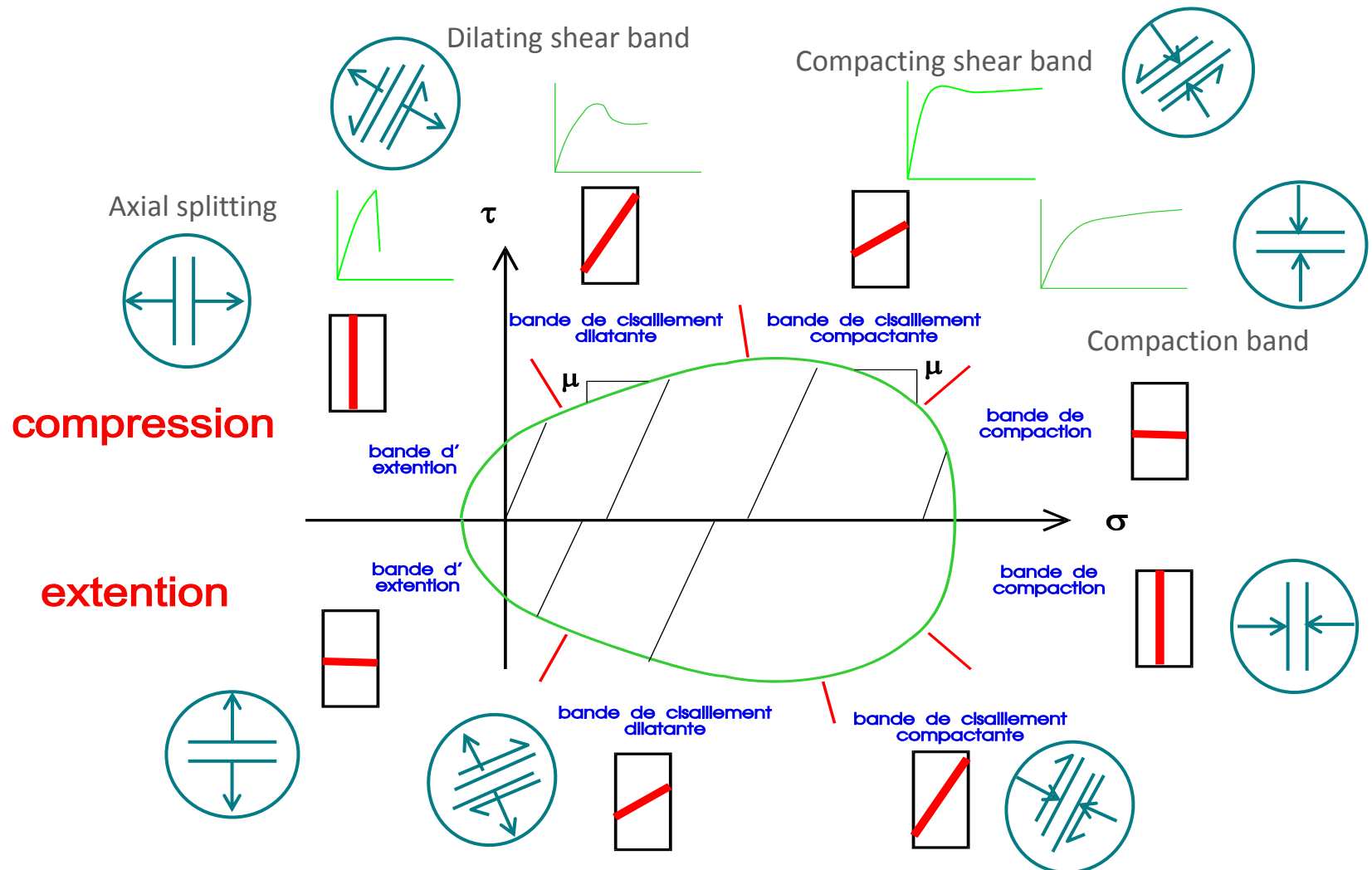


Fig. 14. Microphotographs of a shear band formed in a drained test under 50 MPa of confinement: general view and detail.

from Sulem et al (2006)

# Experimental investigation in rocks

## ➤ Effect of mean stress: synthesis (for porous rocks)

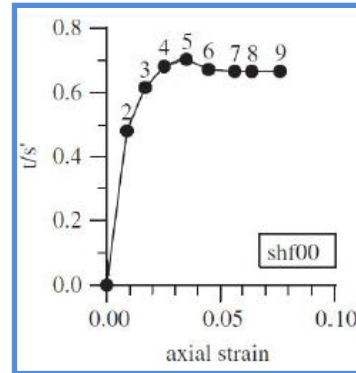
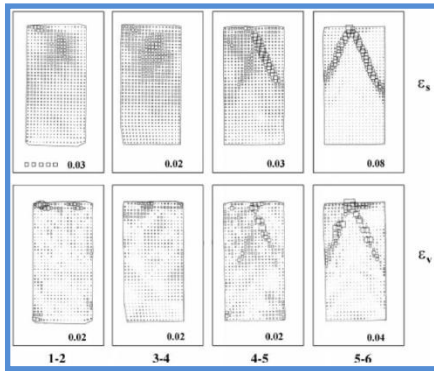




# Outline

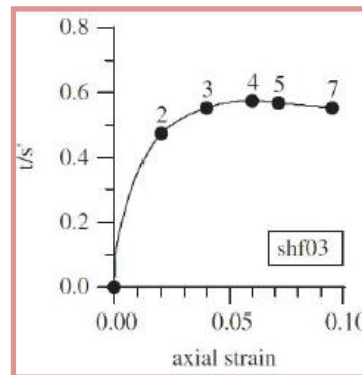
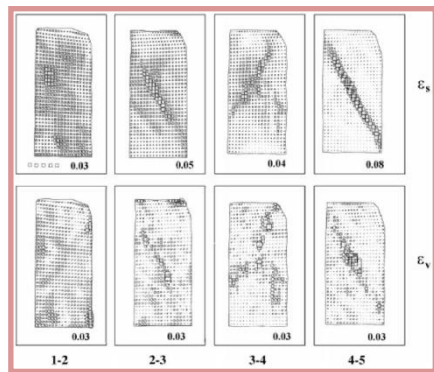
- Introduction
  - *in situ* observations
  - impacts of strain localisation
- Experimental investigations: methods
  - *post-mortem* observations
  - multiple (internal) measurements
  - full field measurements
- **Experimental results (a few)**
  - strain localisation in sands
  - strain localisation in rocks
  - **the emergence of strain localisation in geomaterials**
- Conclusions

# The emergence of strain localisation: sands

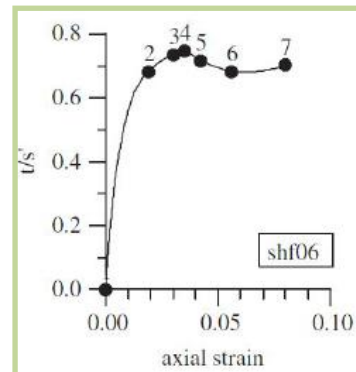
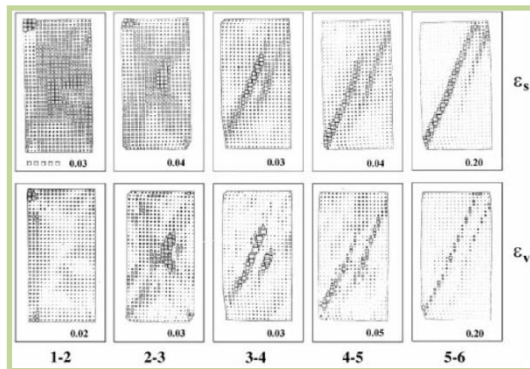


Plane strain compression tests on Hostun sand  
Incremental fields of shear strain measured by *false relief stereo-photogrammetry* (Desrues et al.):

- intermediate state (density)
- mostly dilative inside the shear band



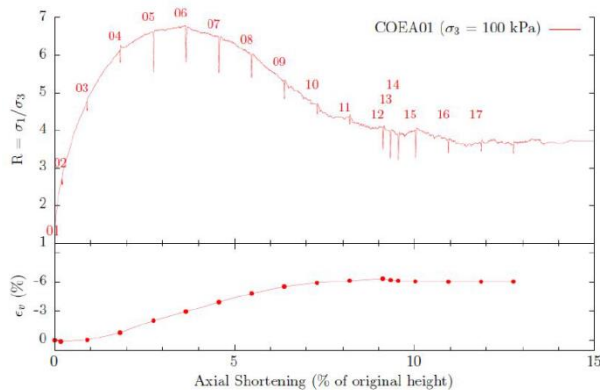
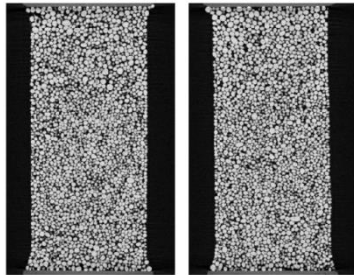
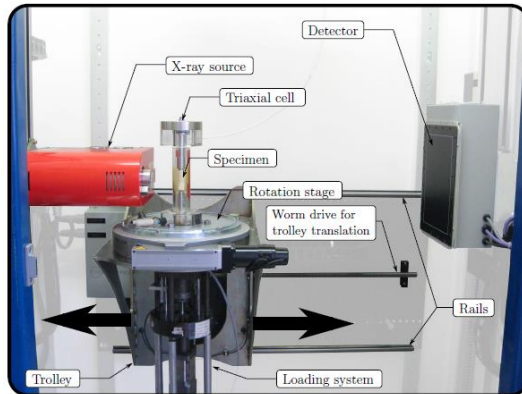
- loose state
- both contractive and dilative incremental behaviors were exhibited inside the band



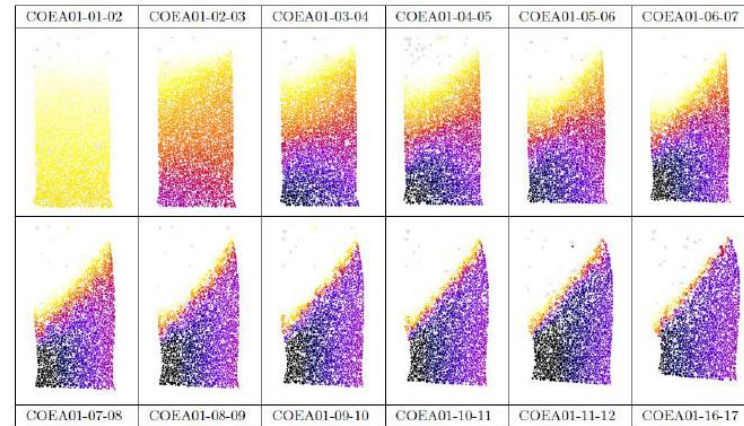
- dense state
- dilative inside shear band

*Is strain localisation an abrupt phenomena ?  
The relative 'low' spatial and strain resolution of  
FRS doesn't allow to respond. Probably not...*

# The emergence of strain localisation: sands

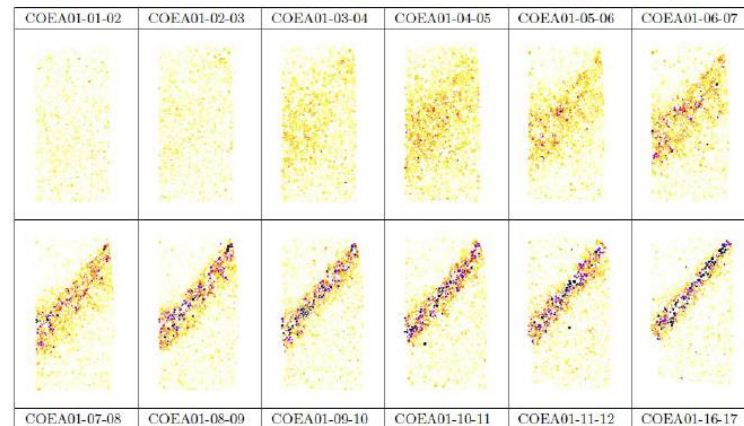


*in situ* triaxial compression tests on Caicos sand  
Incremental fields of grain kinematic measured by  
*X-ray CT* and *discrete V-DIC* (Andò et al.):



*vertical  
displacement*

Vertical Displacement  
 $\geq 0$    
 $\leq -15.4 \text{ px}$   
 $\leq -239.6 \mu\text{m} (\sim 0.5 D_{50})$

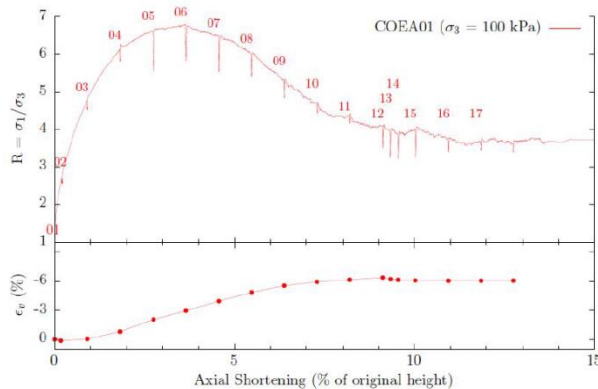
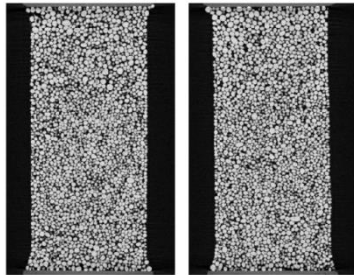
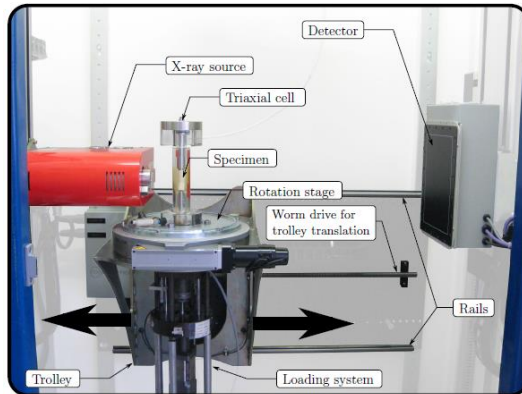


*rotation  
angle*

Rotation angle  
(axis not shown)  
 $0$    
 $\geq 20^\circ$

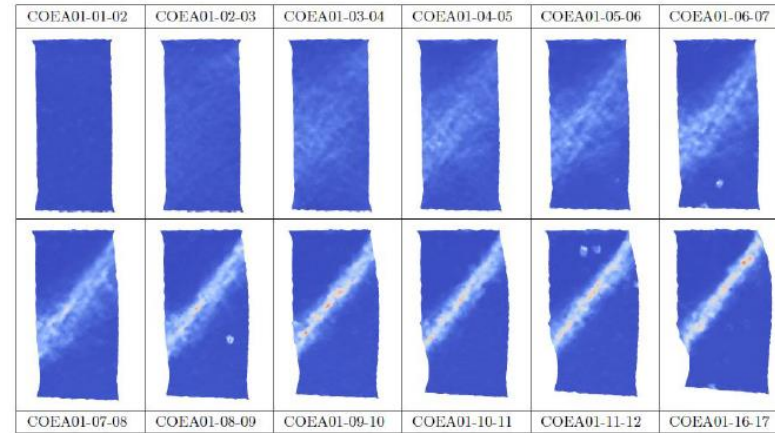


# The emergence of strain localisation: sands



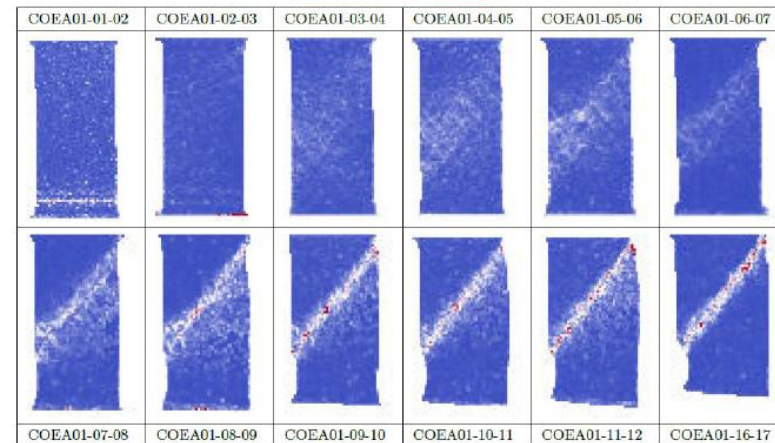
*in situ* triaxial compression tests on Caicos sand

Incremental fields of shear strain measured by *X-ray CT*, *grain tracking* and *discrete V-DIC* (Andò et al.):



*Shear strain (from grain tracking – without DIC)*

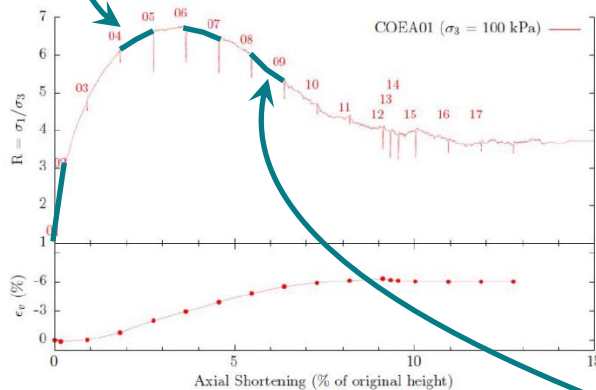
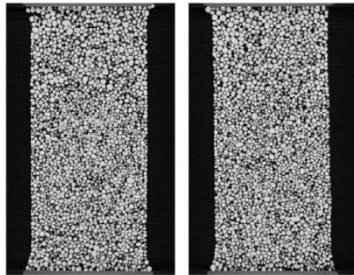
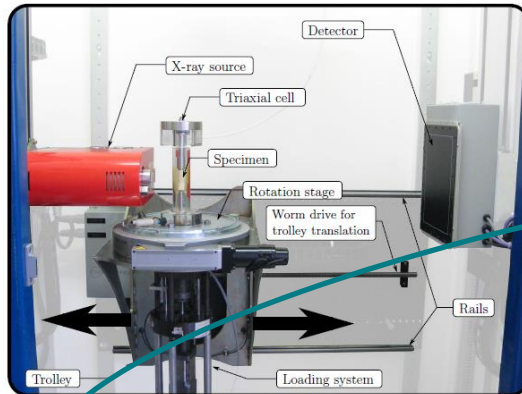
Deviatoric strain  
0 ≥ 0.25



*Shear strain (continuous V-DIC)*

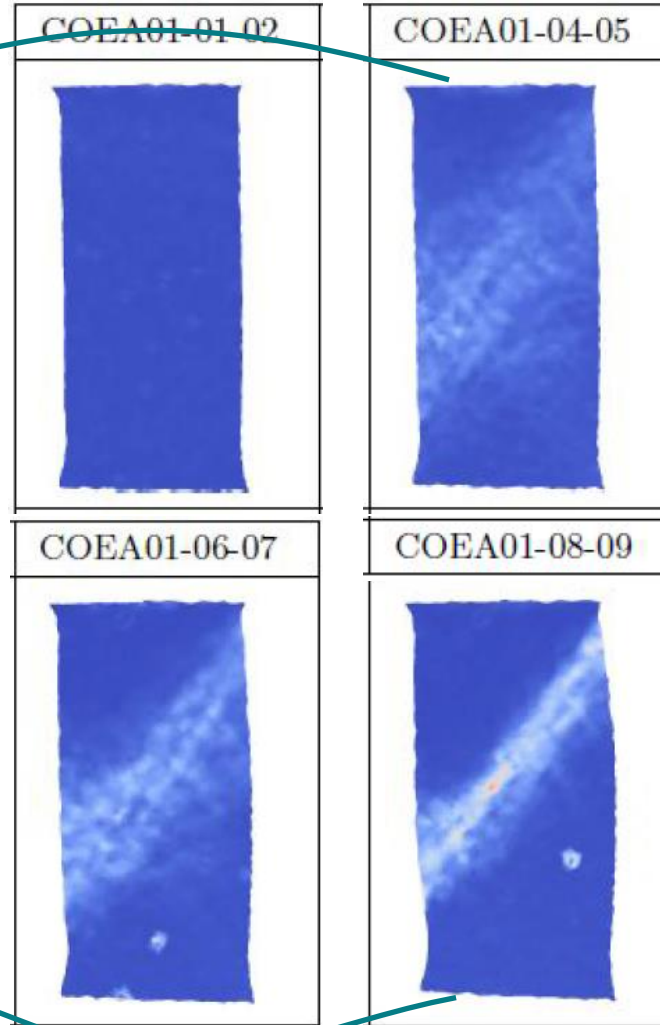
Deviatoric strain  
0 ≥ 0.25

# The emergence of strain localisation: sands



*in situ* triaxial compression tests on Caicos sand

Incremental fields of grain kinematic measured by  
X-ray CT and discrete V-DIC (Andò et al.):



*Shear strain (from grain tracking – without DIC)*

- initial loading: perfectly homogeneous
- before peak: a large zone of strain concentration with a texture like multiple parallel and conjugate bands
- after peak: one main band through the previous zone of strain concentration

*The strain localization appears as a progressive process*

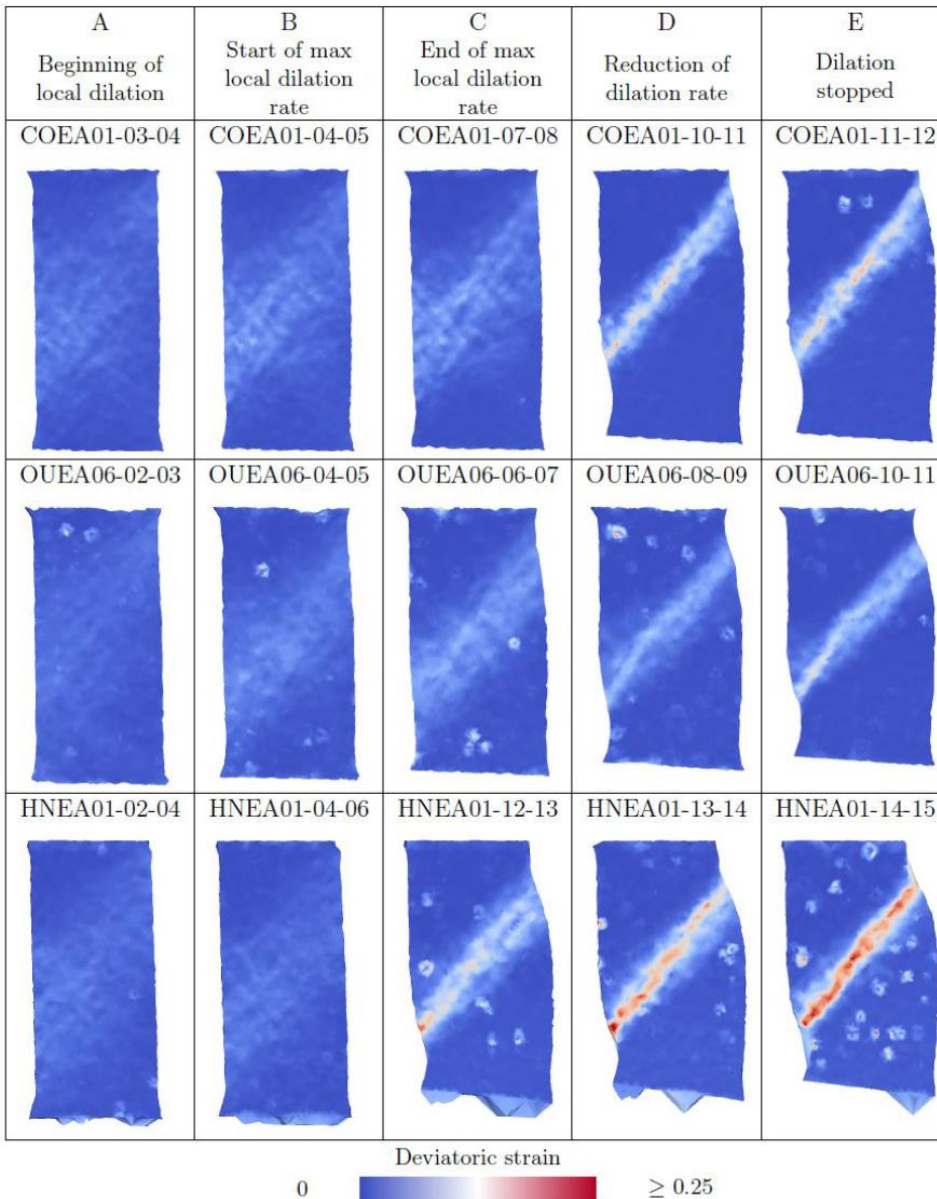


# The emergence of strain localisation: sands

*in situ* triaxial compression tests on three sands  
Incremental fields of grain kinematic measured by  
*X-ray CT* and *discrete V-DIC* (Andò et al.):

- a fine texture of multiple parallel and conjugate bands appears at the beginning of dilation
- the fine texture is reinforced during the dilative regime
- progressively, the pattern become a main shear band. The volume changed is then stopped

*The strain localization appears as a  
progressive process*



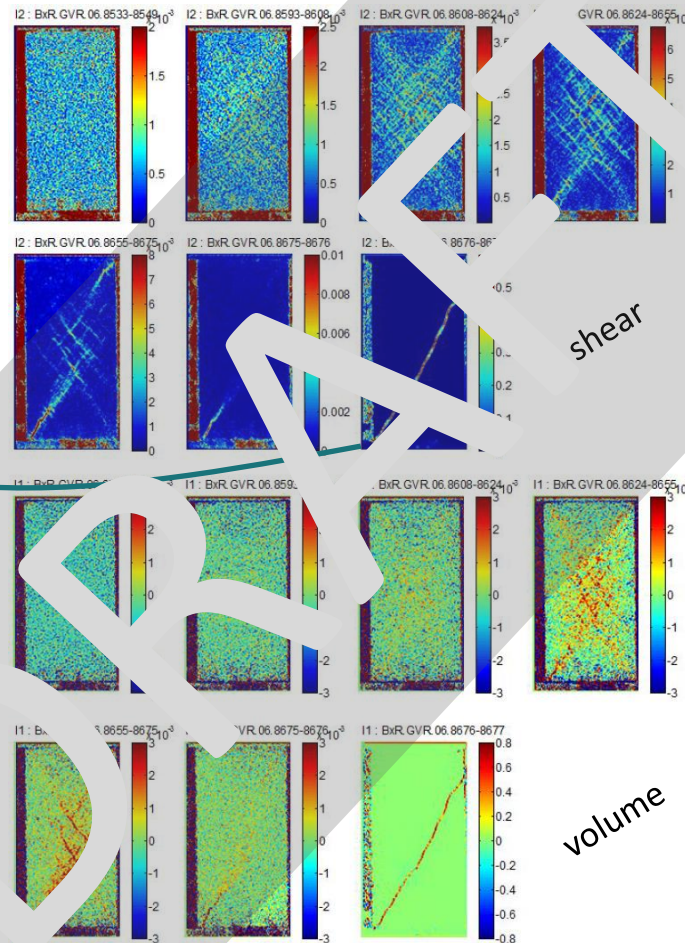
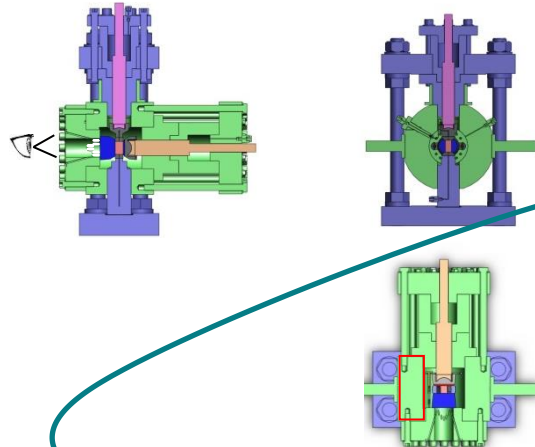


# The emergence of strain localisation: rocks

*in situ* plane strain compression tests on a Vosges sandstone

Incremental fields of shear and volume strain measured by DIC (Lanata et al.):

Confining pressure [MPa]



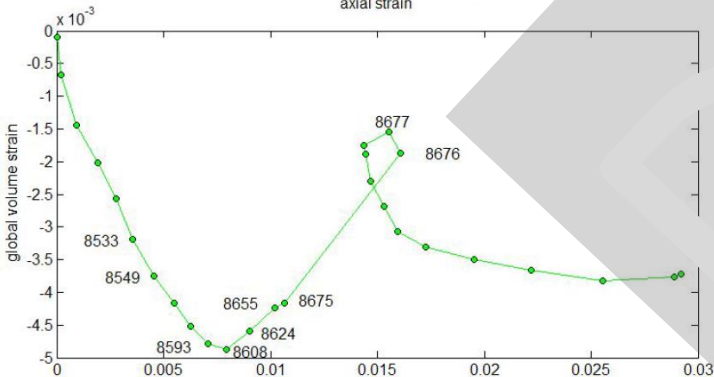
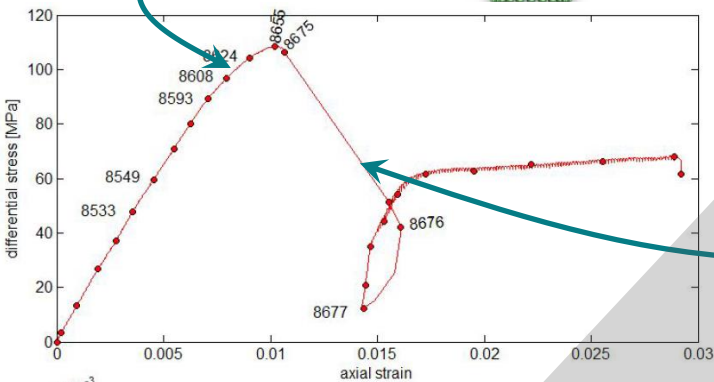
- a fine texture of multiple parallel and conjugate bands appears before the stress peak

- until the peak, some band are de-activated – *natural selection*

- progressively, the pattern become a main shear band after the peak

- deformation inside bands is dilative

*The strain localization appears as a progressive process*

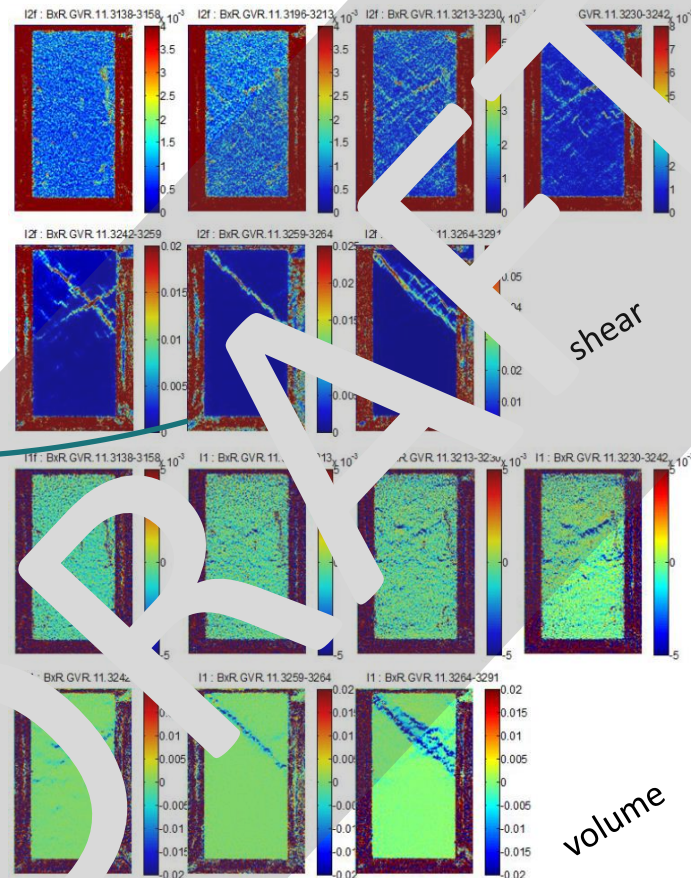
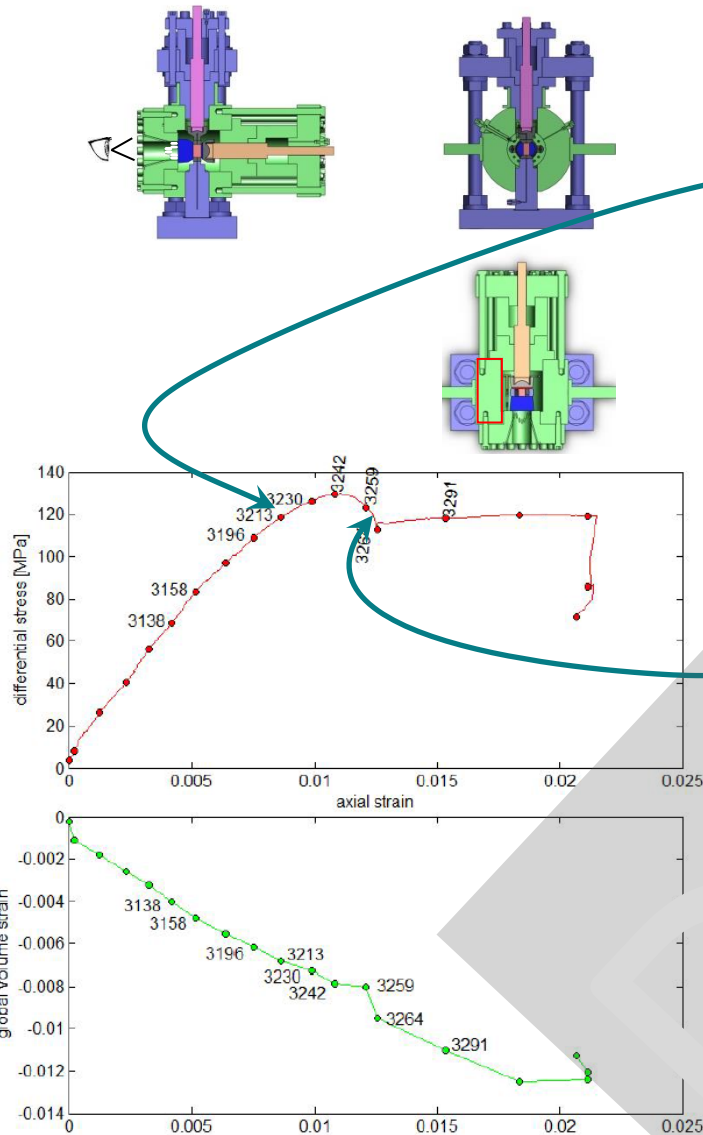


# The emergence of strain localisation: rocks

*in situ* plane strain compression tests on a Vosges sandstone

Incremental fields of shear and volume strain measured by DIC (Lanata et al.):

Confining pressure [MPa]



- a fine texture of multiple parallel and conjugate bands appears before the stress peak

- until the peak, some band are de-activated – *natural selection*

- progressively, the pattern become a main shear band after the peak

- deformation inside bands is compactive

*The strain localization appears as a progressive process*

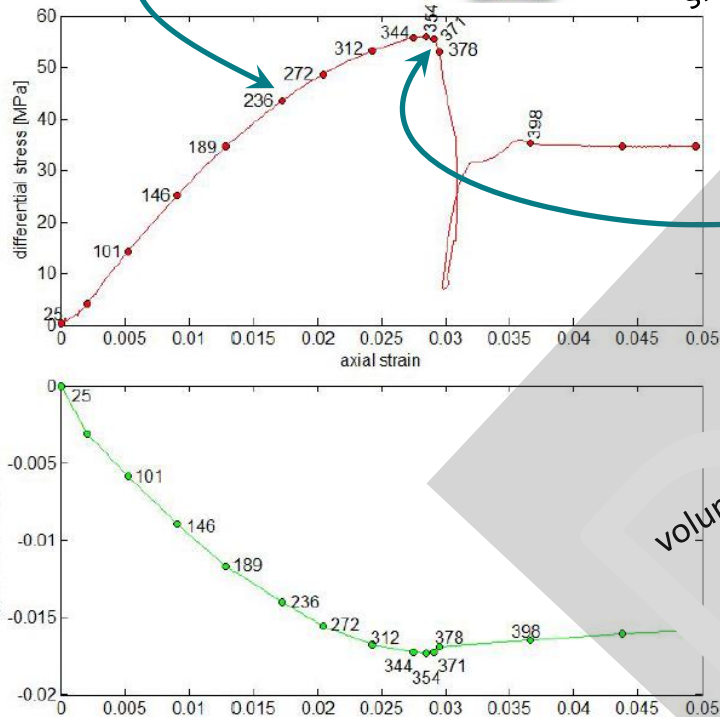
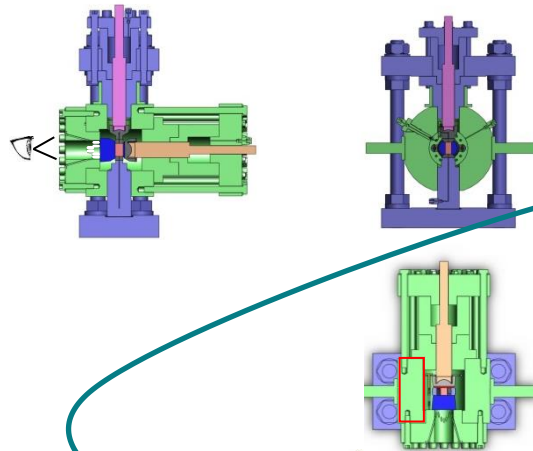


# The emergence of strain localisation: rocks

*in situ* plane strain compression tests on a **clayey stone**

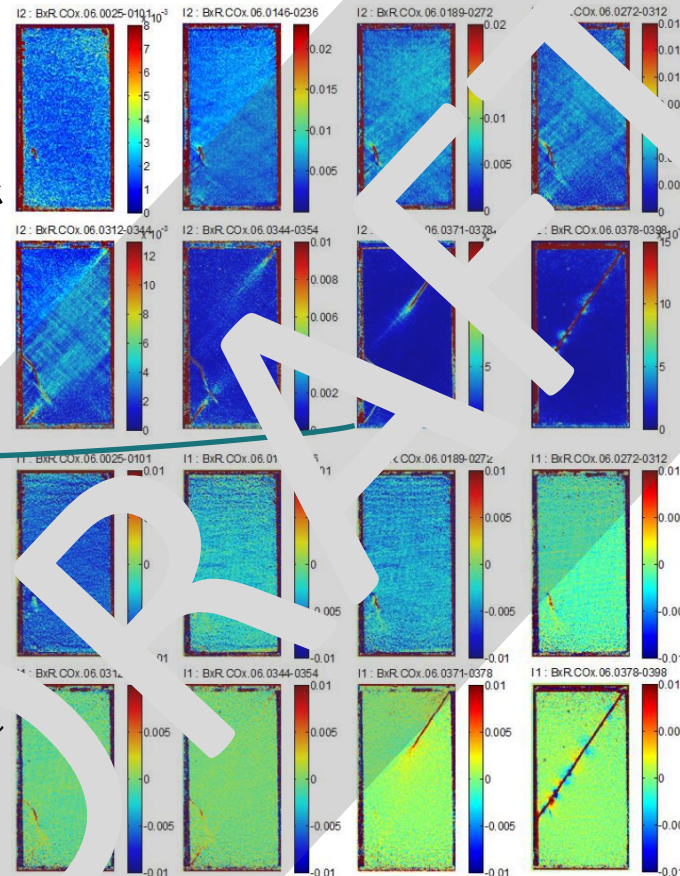
Incremental fields of shear and volume strain measured by *DIC* (Bésuelle et al.):

Confining pressure [MPa]



shear

volume



- a fine texture of multiple parallel and conjugate bands appears before the stress peak
- until the peak, some band are de-activated – *natural selection*
- progressively, the pattern become a main shear band after the peak

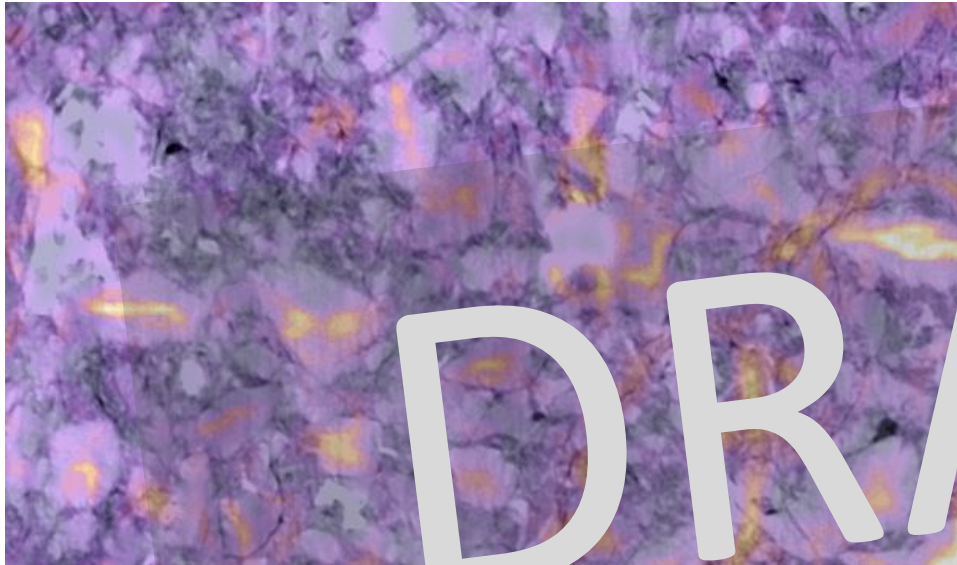
*The strain localization appears as a progressive process*



# The emergence of strain localisation: rocks

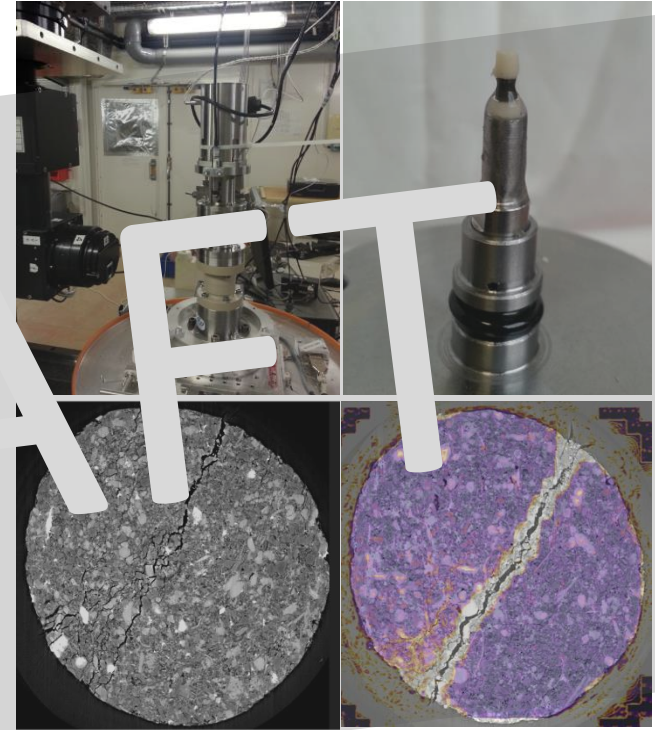
*in situ* triaxial compression tests on a **clayey stone**

Incremental fields of shear strain measured by *DIC* (Bésuelle et al.):



10 $\mu$ m

Overlapping between X-ray  $\eta$  nano-CT and incremental 2<sup>nd</sup> strain invariant field (DIC)

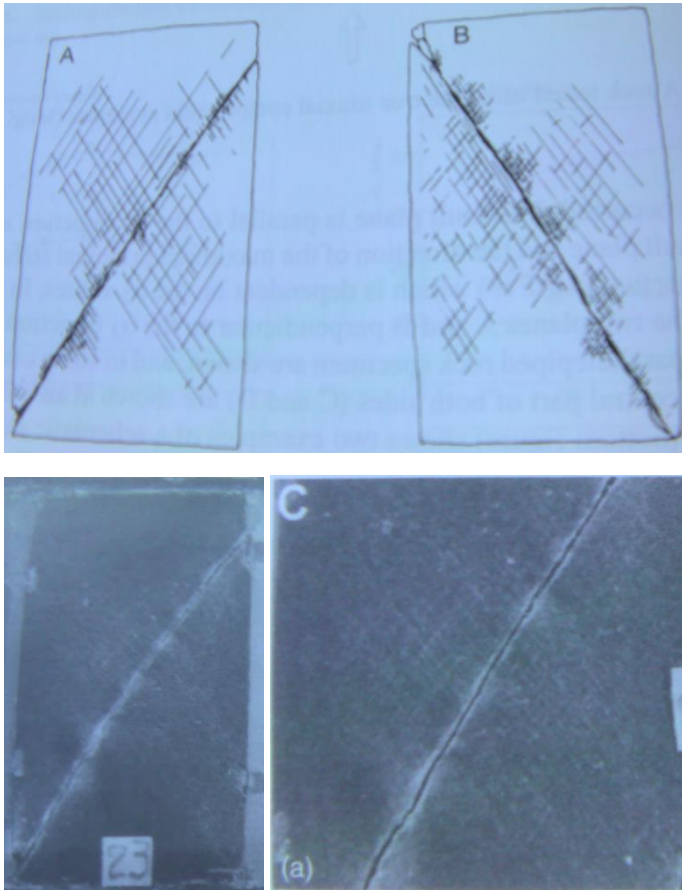


100 $\mu$ m

*In situ* triaxial loading test at ESRF (ID19)  
X-ray nanotomography + volume DIC  
Specimen  $\varnothing$  1.3 mm, H 2.5 mm

# The emergence of strain localisation: rocks

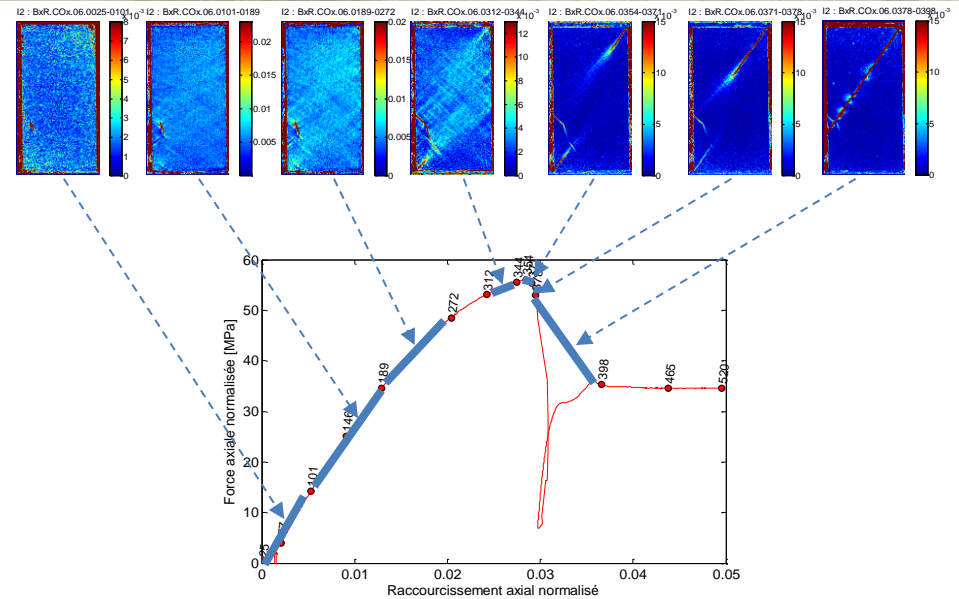
True triaxial compression tests on the Dunham **dolomite**  
*post mortem* observations of the specimens (from Mogi):



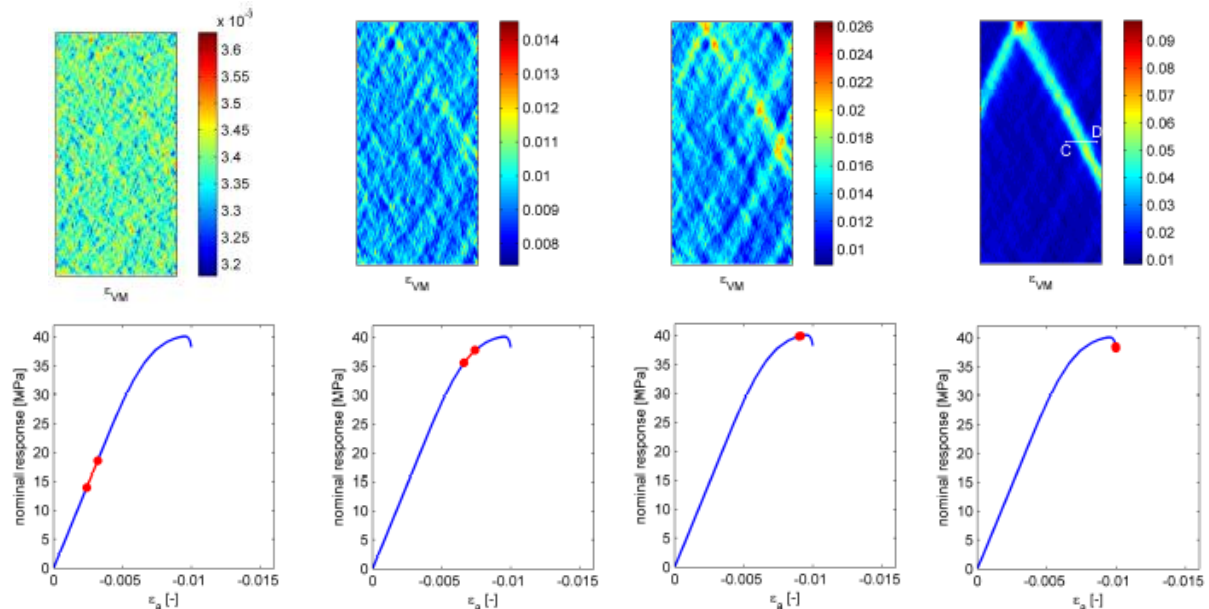
*Evidence of an early strain  
localisation by multiple parallel  
and conjugated shear bands ?*

# The emergence of strain localisation: rocks

What about numerical modeling ?



- a double scale model  
FEM x FEM
- heterogeneity of the VER
- progressively process of strain localisation (PhD thesis, B. van den Eijnden, 2015)





# Conclusions

## ➤ Methods

- *Improvement of the methods during last decades: higher photograph resolution, finer resolution of X-ray CT, Volume-DIC, discrete volume-DIC, new experimental devices, etc...*
- *The improvement of the spatial resolution and the grey-level resolution allows to detect finer and finer details of the regimes of deformation*

## ➤ Experimental investigations of the strain localisation

- *Quasi-general mode of failure in geomaterials (without high temperature)*
- *Reproducibility of some characteristics: shear band orientation, band thickness, kind of deformation inside shear band (compaction/dilation)*
- *Non-reproducibility of some observations: shear band pattern, post-peak response*

## ➤ Experimental investigations of the emergence of localisation

Recent investigations thanks to more advanced experimental devices

- *strain localisation is a progressive process*
- *localisation starts well before stress peak under the form of multiple parallel and conjugated shear bands. Some of these bands are de-activated in the next loading. A few bands keep active after stress peak. Today observed in several sands and rocks.*



# Thank you for your attention



*Field observation of multiple parallel and conjugated shear bands – disused quarry in Orange, France*